Electron spectroscopy

van Pol, J.H.G.

Award date:
1991

Electron Spectroscopy

J.H.G. van Pol

18 october 1991

Het afstudeeronderzoek heeft plaatsgevonden aan het Kernfysisch Versneller Instituut te Groningen. Met dit afstudeerverslag wordt de studie voor Ingenieur in de Technische Natuurkunde aan de Technische Universiteit Eindhoven afgesloten.

Abstract

The development of an electron spectrometer of the Mini-Orange type is described. Particular attention was given to its compactness since the use of it in conjunction with present detector arrays (such as the Nordball at NBI) is envisionage. Tests were performed with sources and in beam.

Results from the measurement of the internal (electron) conversion coefficients of transitions de-exciting high spins states in ^{150}Eu and ^{151}Eu are presented. The ^{148}Nd(^{7}li,xn) reaction was used, at the Tandem accelerator of Orsay - France, to populate these states. The non-observation of strong (enhanced) electric-dipole transitions, implies that these nuclei do not have static octupole deformed shapes at high spins.

Contents

Introduction

The research described in this work was done at the KVI (Kernfysisch Versneller Instituut) in Groningen (the Netherlands). It will be the final part of my study for Physics Engineer at the Technical University Eindhoven.

The aim of this work is twofold. In the first part a description of a Mini Orange type electron spectrometer will be given. The interesting feature of this spectrometer is its small size which enables mounting it in γ-detector arrays where little space is available (like the Nordball). To test the spectrometer, in beam experiments were performed at the Niels Bohr Institute (Denmark), the KVI and in Debrecen (Hungary). Each experiment resulted in changes of the spectrometer design, finally yielding the design as it will be described in part I.

In part II the results of an in beam internal (electron) conversion experiment will be presented. This experiment is an addition to earlier performed $\gamma\gamma$-coincidence and angular correlation experiments, to determine the internal structure of the ^{150}Eu and ^{151}Eu nuclei. The experiment took place in Orsay (France) where a high resolution, low background, electron spectrometer is available. The results from this experiment and the suggested level scheme for the Europium nuclei will be shown in part II.

Part I

MINI ORANGE SPECTROMETER

Chapter 1

Introduction to part I

In this part the results of in beam tests performed with a Mini Orange type electron spectrometer will be presented. The spectrometer was designed to be mounted in the nordball, a γ-ray spectrometer present at the Niels Bohr Institute in Risø(Denmark). The purpose of using a Mini Orange type of spectrometer is its compact design, which is needed to fit the spectrometer in the Nordball as will be explained later. The principle of this spectrometer is a set of permanent magnets placed between the target and the detector making it possible to select electrons of an energy matching the magnetic field of the magnets. In the following chapter a detailed description of a Mini Orange will be given (chapter 2).

Next the features of the spectrometer will be given, including the characteristics of the specially for this spectrometer designed Mini Orange and SiLi-detector (chapter 3).

Finally the results of the tests performed with this spectrometer at the KVI and in Debrecen (Hungary) will be given (section 3.1).

More detailed information about Mini Oranges and there usage can be found in reference [Klinken 1986]. The Mini Orange spectrometer used has been described before in reference [Steenbergen 1989].

Chapter 2

Mini Orange

A Mini Orange consists of a central absorber with wedge shaped permanent magnets mounted around it (figure 2.1). The name of this spectrometer, Mini Orange, originates from the similarity between its shape and that of a small orange.

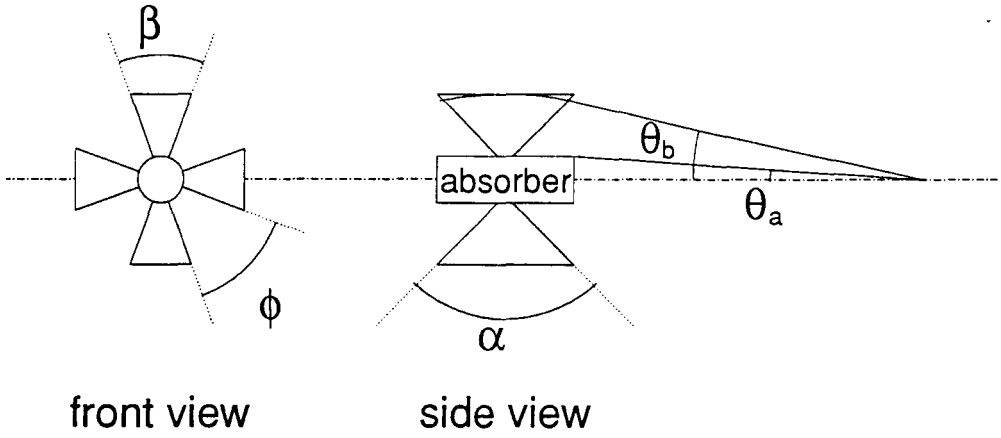

Figure 2.1: *Mini Orange*

The permanent magnets cause a toroidal magnetic field. Charged particles entering this field under an angle θ relative to the central axis feel a force that bends their trajectory back to the central axis. The radius of the curvature depends on the momentum of the particle and on the magnetic field (see below). Neutral particles (particular γ-rays) will not be influenced by the magnetic field. Therefore an absorber is used on the central axis which

is designed to shadow straight line trajectories, from the source, to reach the detector (figure 2.2).

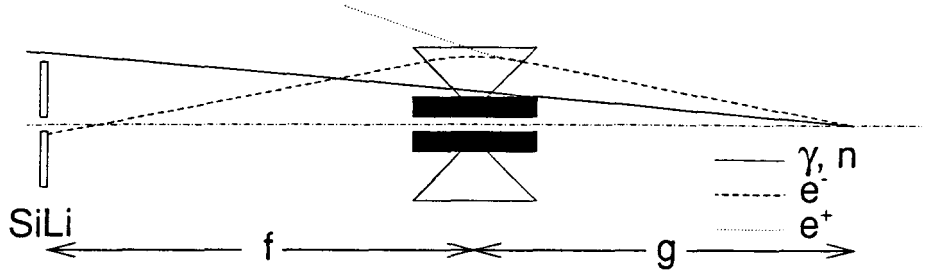

Figure 2.2: *Trajectories through a Mini Orange for different particles*

- For charged particles the Mini Orange works like a lens where the target and detector are the "object" and the "image". Depending on the charge of the particle and the direction of the magnetic field, either negative or positive charged particles will be bend towards the central axis. In the case of this spectrometer the Mini Orange is meant to focus negative charged particles towards the central axis. In more detail the bending of a charged particle in a magnetic field can be described using the equation of motion classically:

$$qvB = \frac{mv^2}{\rho} \tag{2.1}$$

Where q is the charge, v the velocity and m the mass of the incident particle. B is the toroidal magnetic field and ρ is the bending radius due to this magnetic field. However, an electron of 100 keV will have a speed of approximately half the speed of light, which means that a relativistic approach is needed to describe the motion of the electron. In that case we find:

$$B\rho = \frac{E_0}{c}\sqrt{\frac{\beta^2}{1-\beta^2}} \tag{2.2}$$

with $\beta = \frac{v}{c}$. Here E_0 is the rest mass of the electron in units of electron volts ($E_0 = 511$ keV). This equation shows that if a an electron enters

a magnetic field B with a velocity v the bending radius will be fixed. Because of the finite size of the detector a range of incident energies will produce trajectories which hit the detector. By choosing the magnetic field, the source-Mini Orange and the Mini Orange-detector distances, the desired energy window can be selected. In this way the contribution from "background" electrons with energies outside the window of interest will be reduced. One of the main parts of the electron background in beam is due to δ electrons. δ electrons are produced when incident projectiles knock out atomic electrons from the target nuclei. The energy of these δ electrons extends up to (reference [Ejiri 1989]):

$$E(\delta) = 4(\frac{m_e}{m_a}E_k E_a)^{\frac{1}{2}} + 4\frac{m_e}{m_a}E_a \qquad (2.3)$$

Where m_e and m_a are respectively the masses of the electron and the projectile, E_k is the binding energy of the k electron in the target nucleus and E_a is the projectile energy. In the case of the later on described KVI experiment, where a ^{40}Ar beam with an energy of 180 MeV hits a ^{124}Sn target, a value of 44 keV is found for $E(\delta)$ (the binding energy of a k-electron in ^{124}Sn is 29.2 keV). Because of these δ electrons it is very difficult to measure electron peaks with small intensities at low energies.

- Neutral particles will either be stopped in the absorber or strongly reduced in intensity. So the absorber shadows the detector for γ-rays and neutral particles coming from the target.

- If one turns the Mini Orange over 180° it will focus on positive charged particles instead of negative charged particles.

The transmission through the spectrometer for a selected energy window is determined by the limited solid angle, blocking due to the magnets and the efficiency of the detector. The solid angle part of the transmission is determined by a term $\frac{1}{2}(cos\theta_a - cos\theta_b)$. Here θ_a is the minimum angle of acceptance, determined by the size of the absorber and the distance between the source and the Mini Orange g, and θ_b is the maximum angle determined by the size of the magnets and the distances g and f, where f is the distance between mini orange and detector (see figure 2.1 and figure 2.2). Within this solid angle it is presumed that all electrons entering the Mini Orange

reach the detector. However trajectories entering the Mini Orange in those regions where the magnets are placed are blocked. The blocking factor, b, is defined as the ratio of space occupied by the magnets relative to the total: $b = \frac{\beta}{\phi+\beta} \approx \frac{\beta}{\phi}$. So for the transmission equation the term $(1-b)$ is included. Finally there is a correction for those particles that reach the detector but are not detected due to e.g. backscattering. This ratio will be called k, so in the transmission this gives a $(1-k)$ term. The transmission equation based on the above mentioned factors then becomes: (see also figure 3.4)

$$T = \frac{1}{2}(cos\theta_a - cos\theta_b)(1-b)(1-k) \tag{2.4}$$

For the specific Mini Orange used for this spectrometer the blocking factor is approximately 0.06, for k a value of 0.35 for perpendicular entry has been chosen (reference [Steenbergen 1989]) and the angles are found to be respectively 8° and 27° (the distance g is approximately 5 centimeters). The obtained value for the transmission in this case is 4%.

Chapter 3

Spectrometer setup

At the Niels Bohr institute in Denmark a γ-ray spectrometer called the Nordball is present. The Nordball is an assembly consisting of 20 Germanium detectors with BGO Compton suppression shields, which improves the detectors response functions, and an array of BaF_2 scintillators producing the γ multiplicity and the total energy data on an event by event bases. The described Mini Orange spectrometer was specially designed to enable its operation in combination with the Nordball. In particular the constraints on the geometrical size introduced difficulties for the operation of the system (as will be explained later). A detailed description of the development and design of this spectrometer is given in [Steenbergen 1989].

Because the measurements are primarily in beam and from heavy ion induced reactions, Doppler broadening of the spectral lines had to be reduced. To minimize the Doppler broadening the detector angle has to be as close as possible to the beam axis. Since there is a larger background radiation at forward angles (0^o), the spectrometer was designed for operation at 180^o. In this geometry the detector as well as the Mini Orange need to have a central passage for the beam.

The SiLi-detector (figure 3.1) designed for this setup has a diameter of 4.5 cm, a 8 mm hole in the middle and consists of four parts. Actually there are four separate detectors each covering a quarter of the total detector. These separate detectors have a common high voltage but the FETs and preamplifiers are separated for all four. In combination with this SiLi detector a Mini Orange is used, consisting of a central Tungsten absorber and four permanent $SmCo_5$ magnets. $SmCo_5$ has been chosen because it can be cut at

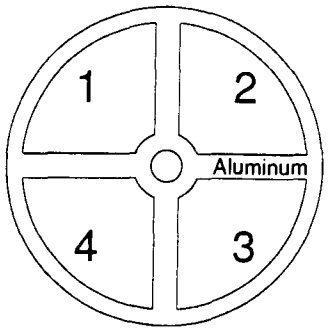

Figure 3.1: *Front view of the SiLi-detector. The detector is separated in four parts labelled 1 to 4. In the text will be referred to these parts as detector 1 to detector 4*

the KVI with a diamond saw. The magnetic field in the Mini Orange varies from 0.2 Tesla close to the magnets, to 0.07 Tesla in between two magnets. Taking four magnets creates a setup where every magnetic gap (the space between two magnets) corresponds to one detector. So for every gap the transmission can be measured instead of measuring one average transmission for the whole Mini Orange.

To improve the energy resolution of the detector it is DC-coupled. Often detectors are AC coupled, this means that a capacitor is placed in between the detector output and the preamplifier input. The advantage of a AC-coupled device is that a DC-offset of the detector does not influence the preampliers. However the disadvantage is that by inserting a capacitor in the circuit the noise also increases so the energy resolution becomes worse. When coupling the system DC this noise is reduced but now it is important to avoid saturation of the preamplifiers due to a high DC offset from the detector. This can be done by cooling the detector (in the case of this spectrometer a temperature smaller than -140 °C is needed). An extra advantage of cooling the detector is that the thermal noise also decreases with decreasing temperature. Because there is no place inside the Nordball to mount a dewar, containing the liquid nitrogen to cool the detector, it has to be placed outside and a cold finger makes the connection between the dewar and the detector.

The final spectrometer design is shown in figure 3.2. There is on feature one can not see from the picture. It is possible to change the distance between the Mini Orange and the target and the distance between the Mini Orange and the SiLi-detector.

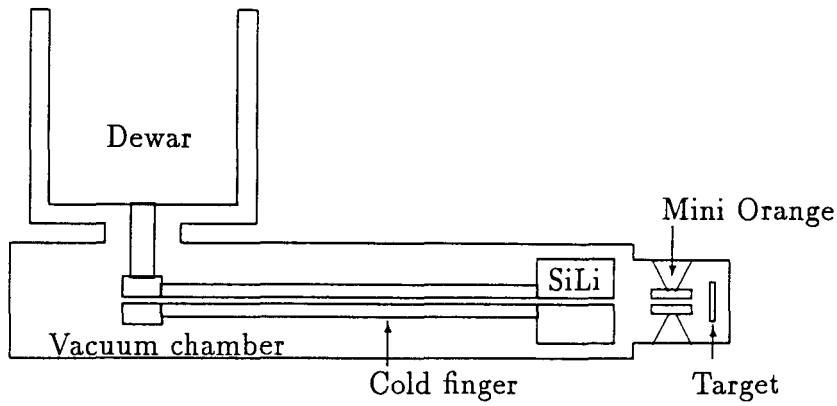

Figure 3.2: *Schematical drawing of the Mini Orange Spectrometer*

3.1 Performed tests

Before doing in beam experiments with the Mini Orange spectrometer tests with sources were done. These tests are split in two parts. In the first part a continuum electron source (^{106}Ru, see figure 3.4) was used to determine the transmission of the Mini Orange. In the second case a discreet electron source (^{207}Bi, see figure 3.3) was used to determine the energy resolution of the SiLi-detector.

During the tests with the discreet electron source the Mini Orange was removed from the setup to make sure that the energy resolution measured is actually the energy resolution of the SiLi-detector and not influenced by the Mini Orange. The best resolutions found for the 4 separate detectors at 1 MeV are listed in table 3.1. These are resolutions determined by fitting

Detector	1	2	3	4
FWHM (keV)	2.84	3.06	3.26	3.01

Table 3.1: *FWHM measured using a ^{207}Bi source*

the electron peaks with a pure Gaussian and neglecting the fact that there exists a low energy tail. The tail can be caused by energy straggling when

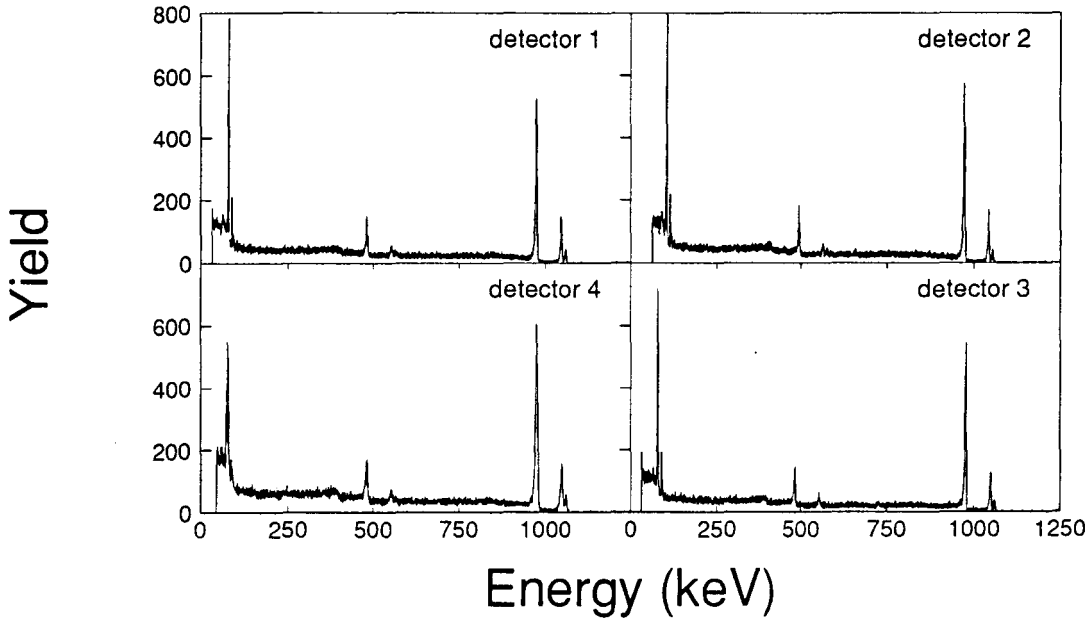

Figure 3.3: *Spectrum measured using a ^{207}Bi source*

th electrons go through a dead layer of the detector, or a layer at the source. A better fit might show that the actual resolution is better. It needs to be noted that the measured resolution is sensitive to the type of spectroscopic amplifiers being used (in the next chapter this sensitivity will be explained in more detail). For these tests Ortec 572 spectroscopic amplifiers were used with the time constant set to $3\mu s$.

The tests performed to determine the transmission of the Mini Orange are done in two parts. First a measurement without Mini Orange was performed and after that a measurement with Mini Orange in between source and detector. The transmission as shown in figure 3.4 has been normalized to 1 for the maximum transmission. The transmission varied actually over the 4 detectors which was mainly caused by the shape of the source which could not be mounted in such a way that it would be symmetrically around the center. Figure 3.4 shows that there is a low energy cut off starting at

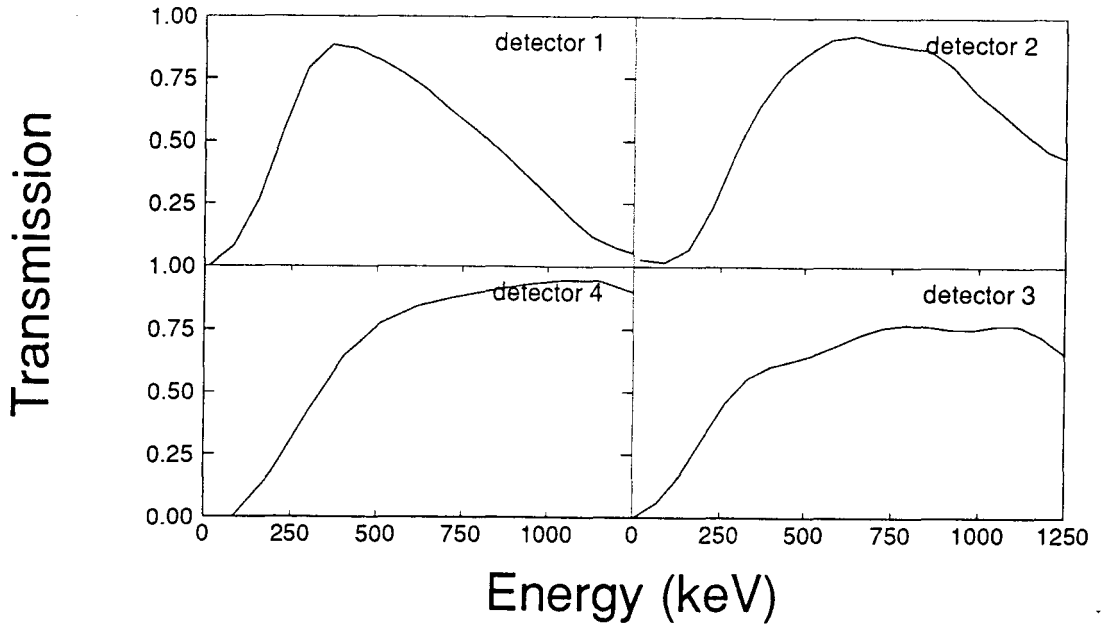

Figure 3.4: *Spectrum measured using a* ^{106}Ru *source*

100 keV, so the number of low energetic delta electrons is reduced. There is also a high energy cut off which is very clearly visible for detector 1. For the other detectors this cut off is at higher energies (around 1.5 MeV). Another explanation for the differences in the transmission curves is the quality of the magnets. These magnets are home made and the procedure does not allow it to determine precisely the field in the magnets. So differences in the curves are partly due to different magnetic fields between the magnets.

Chapter 4

Solved and unsolved problems

Though the title may seem a little bit strange it is the most appropriate one. The meaning of this section is to give an overview of the problems that occurred during in beam experiments with the experimental setup as shown in figure 3.2. Partly these have been solved and the method will be explained. However still some problems are left and an illustration of these might enable other people to improve the setup.

- As mentioned earlier one of the biggest problems to operate this setup is the temperature of the detector. If the temperature is too high (greater than -140°C) the detector leakage current will be to large which will first saturate the preamplifiers and at even higher temperatures the FETs will be damaged. To make sure that the temperature of the detector becomes less than -140°C it is necessary to have:

  - a good heat conductivity between the dewar and the detector
  - a good vacuum to avoid heat loss due to convection

  For the nitrogen supply an automatic cooling system was designed. This system fills the dewar at preset intervals. The dewar has two hoses connected to it, the first one to fill and the second one to check if the dewar is full. At the end of the second one a sensor is mounted. Only when at this point liquid nitrogen is seen the cooling system will stop filling the dewar. For security reasons a maximum filling period is set, so when after a preset time still no liquid nitrogen has reached the sensor it is presumed that something went wrong, then the filling

stop and the module gives an alarm. The vacuum and temperature conductivity have caused no problems during all the performed tests. The vacuum reached every time the same value (10^{-5} mbar) which was found to be satisfactory and also the conductivity gave no problems. However, after cooling 5 or 6 times the cooling procedure took more and more time and the end temperature became worse (a good operating temperature is $-160°C$). The origin of this problem was the construction of the dewar, to connect it to the cold finger a small pipe was made with a small hole in the middle. When one inserts the liquid nitrogen into the dewar it will condensate the water out of the air that is in the dewar. This water will fill up the hole after a while and freeze. Because ice does not conduct very well at low temperatures an isolation layer is created. So the solution was quit simple, after a few times cooling one has to dry up the inside of the dewar.

- Looking at the electronics the sensitivity to external sources and internal cross talk causes major problems. First off all some explanation about the configuration (figure 4.1).

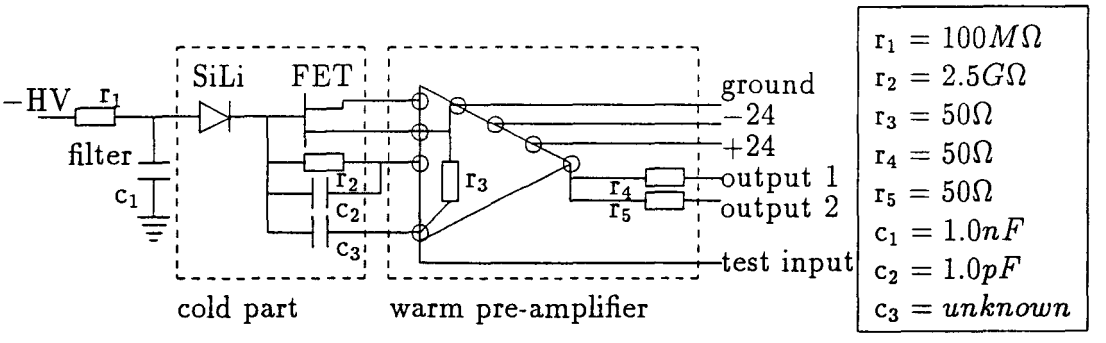

Figure 4.1: *Electronical circuit, the two parts in the dashed boxes are separate for every detector*

On the backside of the detector four FETs are mounted which do the first amplification. They are mounted as close as possible to the detector to avoid pick up of signals from surrounding equipment. These FETs are cooled down together with the detector, since they are mounted

against it, therefore reducing the thermal noise. The FETs are connected to four 'warm' preamplifiers that are specially designed for this detector. The output of the preamplifier is suitable for spectroscopic amplifiers or timing filter amplifiers. The main problem with this system is noise from the electrical equipment around the detector. This means that all devices that are not needed have to be disconnected. To reduce the AC noise coming from the electronics crate and the high voltage supply a low pass filter is mounted between the high voltage supply and the detector. Finally the preamplifiers are very sensitive to oscillations. Part of the reason for these oscillations is cross talk. Because the signal wires for the different detectors are close to each other the signals can influence each other. So when one preamplifier is oscillating, the others will also start to oscillate. To avoid this all unused connections of the preamplifiers have to be terminated with 50 Ω.

4.1 Performed experiments

The described setup (figure 3.2) has been tested in beam three times. On all three occasions there were no actual results. The first of the three experiments was done at the Niels Bohr institute in Risø(Denmark), see [Steenbergen 1989]. In this experiment problems concerning the design were encountered. The main problems and their solutions will be listed here briefly because the experiment was done previous to this work.

- Cross talk was one of the worst problems particularly when working with a lot of signal cables that have to be close to each other for mechanical or other reasons. Originally the signal cables for all four detectors were placed next to each other. Later on four rods were made and mounted with a ground connection, to prevent cross talk.

- Cooling. The dewar designed for this spectrometer was very small with the disadvantage of having to fill very often. A new, and bigger, dewar was designed which increased the filling interval with a factor of three.

- Heating. To open the spectrometer the SiLi-detector has to be warmed up to a temperature above 0°C, otherwise the detector will function

as a cold trap and collect dirt out of the air. This warming procedure takes very long (order of 10 hours) because of the vacuum. The original idea was to use a heating spiral around the cold finger to decrease the time needed to warm up. However during the heating a lot of dirt was set free from the spiral and the surrounding materials. So the spiral was removed again and the warming up procedure was done with the help of nitrogen gas. Breaking the vacuum with nitrogen gas keeps the detector clean and increases heat transport. The warming up period has been lowered to 3 hours with this method.

- Faraday cup. The last problem was the background due to scattering of the beam on the faraday cup. For this reason an extension to the spectrometer was made and the Faraday cup was placed more down stream, so further away from the detector.

The second experiment took place at the KVI (Groningen) where the Dutchball was available. The dutchball is a configuration consisting of 6 Ge detectors with anti Compton BGO shields, 1 X-ray detector and a multiplicity filter of 6 BaF_2. All these detectors are located inside a ball as the name already suggests. The Mini Orange spectrometer was placed under 180° relative to the direction of the beam. The reaction chosen to test the setup was:

$$^{124}_{50}\mathrm{Sn}(\ ^{40}_{18}\mathrm{Ar},\ \mathrm{xn})\ ^{164-xn}_{68}\mathrm{Er}$$

Where the beam energy was 180 MeV and the target had a thickness of 5 mg/cm^2. Before starting the experiment the system was mounted and tested with sources. These tests all gave good results, so the detector worked. The main problem arose with the beam. As mentioned earlier the beam has to pass through the cold finger and the Mini Orange, which means that it has to pass through a hole of 6mm over a length of 750mm. Actually the hole is even a bit smaller because in front of the cold finger and in front of the Mini Orange two collimators are mounted with a smaller diameter (approx. 4mm). The highest current reached during the experiment was 0.1nA at the target. To make this number a bit more clear we can look at the count rate with beam relative to the count rate without beam. When the beam was on, there were two times the number of counts compared to when the beam was off. So the actual signal to background ratio was too small to obtain

any significant statistics. It should be noted at this point that the cause for measuring no spectra was not a failure of the SiLi-detector but a failure in getting enough beam current at the target.

Finally the most recent test was performed at the Atomki institute in Debrecen (Hungary). The basic idea was the same as the KVI experiment. So the spectrometer was mounted under 180° relative to the beam direction. A different reaction was chosen for this test:

$$^{107}_{47}\mathrm{Ag}(\,^{4}_{2}\alpha,\,\mathrm{n})\,^{110}_{49}\mathrm{Nd}$$

The beam energy was 17.5 MeV and the target thickness was 1030 μg/cm^2. Also in this case the test of the setup with source went well, spectra were measured with a resolution of 2,7 keV at 1 MeV. This time the problems were caused by the detector. After replacing the source with the target the detector showed a short circuit. Then the system was warmed up again and during this warming up there were regular tests to see if the short circuit was temperature dependent. This appeared to be the case because for temperatures higher than -90°C there was no short circuit anymore. So probably the short circuit is due to different expansion coefficients which ground the detector for very low temperatures. This made it impossible to perform tests with the detector so the decision was made to cancel the experiment without actually having had beam on the target. In this case it was the SiLi-detector that caused the problem and not the beam current.

At this moment the status of the detector is still the same as described in the Debrecen experiment, so there is still a short circuit and it is not operational.

4.2 Specifications about detector and setup

To end this chapter it might be convenient to give some specifications about the setup that enable other people to operate it more easily. The main numbers will be listed in the table 4.1 below.

Topic		Specifications
General	Temperature	Best $-163°C$
		highest cooling speed: 160° in 2 hours
	Pressure	Best 10^{-5}mbar
Detector	High Voltage	max:-250 Volt
	Resolution (*)	Specifications: 1.7 keV
		measured: 2.7 keV (at 1 MeV)
	Fall time	Specifications: $1 < t_{fall} < 100$ ms
	Rise time	Specifications: $30 < t_{rise} < 50$ ns
	DC offset (**)	Measured: $\approx$20mV

Table 4.1: *Specifications of the detector found by tests and given by the maker of the detector*

(*)To obtain a good resolution the first thing one has to check are the preamplifiers. The specially designed preamplifiers have three adjust knobs. Two of them change the integration and differentiation time, the other one changes the DC offset. For the DC adjustment see '(**)'. The adjustment can be best performed when looking at the signals coming from the detector. With the two knobs one has to make sure that the oscillations are minimized. If this is the case and the DC offset is good (in the order of 5 millivolts) then the preamplifiers are well adjusted.

(**)The DC offset is one of the most important adjustments of the detector. To operate the system it is necessary the check this offset without high voltage on, the offset should then be in the order of millivolts. If this is not the case one has to adjust this with the DC adjust knob. When the high voltage is put on the DC offset should still be low (in the order of 10 millivolts). If this is not the case one has to repeat the described procedure.

Part II

EUROPIUM

Chapter 5

Introduction to part II

In this part the results of an internal (electron) conversion experiment will be presented. This experiment is part of a group of experiments to determine the internal structure of the ^{150}Eu and ^{151}Eu nuclei. The interest in these nuclei originates from the fact that theory suggests that these nuclei are octupole deformed. A review of nuclear deformation is given in chapter 6.

Until now $\gamma\gamma$ coincidence measurements and angular correlation measurements have been performed. These experiments yield information on cascade transitions and the multipole order of a transition. The internal conversion experiment adds an extra feature these data, being the parity change of a given transition (section 6.2). So a combination of the results from the $\gamma\gamma$ coincidence measurement, the angular correlation measurement and the internal conversion measurement makes it possible to suggest level schemes for the two Europium nuclei.

During this experiment the Europium nuclei were produced by bombarding a Neodymium target with Lithium.

$$^{148}_{60}\mathrm{Nd}(\,^{7}_{3}\mathrm{Li} + 50\mathrm{MeV}, 5\mathrm{n})\,^{150}_{63}\mathrm{Eu}$$
$$^{148}_{60}\mathrm{Nd}(\,^{7}_{3}\mathrm{Li} + 40\ \mathrm{MeV}, 4\mathrm{n})\,^{151}_{63}\mathrm{Eu}$$

The experiment was done in Orsay (France). There a high quality ^{7}Li beam is available from the Tandem van de Graaff accelerator, as well as the electron spectrometer which is suitable for this experiment (chapter 7). Finally the results of the experiment will be shown and interpreted in chapter 8.

Chapter 6

Theory

When a projectile nucleus hits a target nucleus with high enough energy fusion becomes possible. The compound nucleus created is, after equilibration of the incident energy and momentum, in an instable state with high energy and angular momentum. One degree of freedom to absorb this energy is collective rotation which immediately implicates that the nucleus is deformed (only in nuclei with a nonspherical equilibrium a rotational motion is allowed in quantum mechanics). One well known type of deformation is the quadrupole deformation where the nucleus is either prolate (cigar like shaped) or oblate (discus like shaped). Quantum mechanically the energy of such a rotating object behaves like:

$$E(I) = \frac{\hbar^2}{2J} I(I+1) \tag{6.1}$$

Where J represents the moment of inertia in units of $\frac{\hbar^2}{MeV}$ and I the angular momentum. So increasing the angular momentum corresponds to increasing the rotational energy. The nuclear excited states form in this case a sequence called Rotational Band. The energies emitted from the decay of such a rotational band are:

$$E_\gamma(I) = \frac{\hbar^2}{2J}(4I-2) \tag{6.2}$$

For an octupole deformed nucleus the situation is slightly different. The idea is that an octupole deformed nucleus has a pear shape, so center of mass (triangle) and center of charge (circle) are shifted relative to each other. This shape can be described with the deformation parameters β_2 and β_3 where β_2

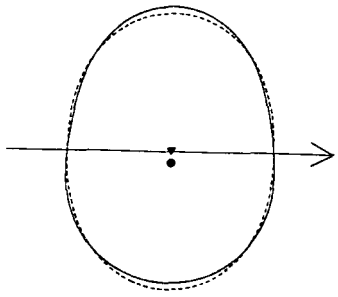

Figure 6.1: *Octupole deformed nucleus with β_2=0.3 and β_3=0.08*

gives the relative strength of the quadrupole deformation and β_3 the relative strength of the octupole deformation. In figure 6.1 the dashed line shows a nucleus with only a quadrupole deformation term that is symmetric to the drawn axis. When including an octupole deformation term one can see that the symmetry disappears. The protons in the nucleus will try to get as far as possible from each other so in the thicker part (below the drawn line) more protons will be present. When such a nucleus starts to rotate around the center of mass (the drawn axis), the center of charge rotates around this axis, so it behaves like an electrical dipole. This means that detecting strong electrical dipole transitions (E1) is an indication for an octupole deformed nucleus. However there are also rotational bands in an octupole deformed nucleus so a spectrum should also show electrical quadrupole transitions (E2). Electromagnetic transitions are explained in more detail in section 6.1. Looking at figure 6.2 one can see such a structure with strong E1 transitions between the bands and strong E2 in band transitions. This structure is a necessary but not sufficient prove that the nucleus is octupole deformed.

As mentioned above the indications for a certain structure of the nucleus are given by detecting the electro-magnetic radiation coming from the decay of the excited nucleus. Until now this has been done via the $\gamma\gamma$ coincidence method. With this method one takes a γ ray of a certain energy and looks which γ rays are detected in coincidence. However the $\gamma\gamma$ method has a limit because it gives no information about the multipole order and the spin change of the transition. For this reason angular correlation measurements have been done. In angular correlation measurements one looks at a cascade of two γ rays. The angle between these two γ rays can be described as a function of the spin and angular momentum of the involved states. This

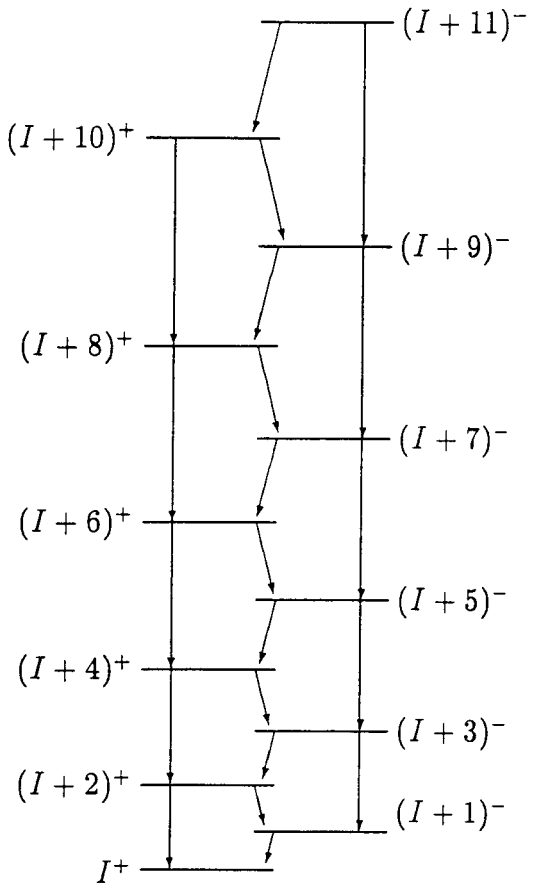

Figure 6.2: *Example of two rotational bands in an octupole deformed nucleus*

correlation is described as (see [Segre 1959]):

$$W(\theta) = \sum_{n=0}^{L} A_2 n P_2 n(cos\theta) \tag{6.3}$$

The coefficients A_L are determined by the angular momentum, and the spin change between the initial and the final state. The values for $W(\theta)$ are known for the different multipolarities. So from measuring $W(\theta)$ one can determine the multipolarity of a transition. However still one can not see the difference between electric and magnetic transitions of the same multipole order. For this reason internal conversion measurements are done. In an internal con-

version experiment one can in principle distinguish electric transitions and magnetic transitions. In section 6.2 this will be discussed in detail.

6.1 Electro-magnetic transitions

Electro-magnetic decay (γ decay) can be evaluated in terms of multipole moments. With a multipole moment the type of transition is described (electric or magnetic) and the multipole order. Equations for the single particle excitation transitions probabilities can be found in reference [Krane 1987]. For the most common transitions the transition probability will be given.

$$\lambda(\mathrm{E1}) = 1.0 \cdot 10^{14}\ A^{\frac{2}{3}} E^3 \qquad \lambda(\mathrm{M1}) = 5.6 \cdot 10^{13}\ E^3$$
$$\lambda(\mathrm{E2}) = 7.3 \cdot 10^{7}\ A^{\frac{4}{3}} E^5 \qquad \lambda(\mathrm{M2}) = 3.5 \cdot 10^{7}\ A^{\frac{2}{3}} E^5$$
$$\lambda(\mathrm{E3}) = 34 \cdot A^2 E^7$$

λ is here in units of s^{-1} and E in units of MeV. From these transition probabilities a few interesting aspects can be deduced:

- First a remark about the validity of the above given equations. As stated these are correct in the case of single particle excitation. So one particle changes its wave function. In real life however one has to consider collective behaviour, which means that all the present particles can change wave function. Because of this the actual (collective) excitation probabilities are approximately 200 times larger.
- These equations show that for energies around 1 MeV the E1 transition ratio is larger than the E2 transition ration. Experimentally however it has been proven that the E1 transition probability is suppressed with a factor of 10^{-4}.
- The transition probability is proportional to E^{2L+1}.
- The transition probability decreases with increasing change of angular momentum.
- Electric transitions are for the same multipole order enhanced compared to magnetic transitions.

Furthermore the decay from a level I_i to a level I_f is limited by angular momentum and parity selection rules. These selection rules are:

$$|I_i - I_f| \leq L \leq I_i + I_f \text{ (no } L = 0)$$

$\Delta\pi = +1$: even electric, odd magnetic
$\Delta\pi = -1$: odd electric, even magnetic

6.2 Internal conversion

When a nucleus is in an excited state it will first de-excite via the emission of nucleons. When the excitation energy has become smaller than the energy needed to emit a nucleon the de-excitation will take place in an electro-magnetic way. There are two modes of electro-magnetic decay.

- Emission of γ rays. The energy of the γ will be equal to the difference in energy of the initial state (E_i) and the final state (E_f) minus the recoil energy of the atom.

$$E_\gamma = E_i - E_f - E_{rec} \tag{6.4}$$

  For $I_i = I_f = 0$ this mode is forbidden. The recoil term in this expression is negligible small (for a γ ray of 1 MeV the recoil energy is less than 100 eV).

- Emission of an electron. The electron energy will be equal to:

$$E_{e^-} = E_\gamma - B_{e^-} \tag{6.5}$$

  where B_{e^-} is the binding energy of the electron.

Now the internal conversion coefficient α is defined as the probability for electron emission (λ_e) relative to that of γ emission (λ_γ).

$$\alpha = \frac{\lambda_e}{\lambda_\gamma} \tag{6.6}$$

For a further understanding it is worthwhile to look at the theoretical equation for α. The actual theoretical description of α is rather difficult, however

one can get an idea how α depends on energy and multipolarity using a nonrelativistic calculation for the electric (E) and magnetic (M) multipoles [Krane 1987]. The derivation of this formula is shown in [Blatt 1966] and for a more exact calculation [Siegbahn 1964] is very suitable.

$$\alpha(EL) \cong \frac{Z^3}{n^3}\left(\frac{L}{L+1}\right)\left(\frac{e^2}{4\pi\epsilon_o\hbar c}\right)^4\left(\frac{2m_ec^2}{E}\right)^{L+5/2} \tag{6.7}$$

$$\alpha(ML) \cong \frac{Z^3}{n^3}\left(\frac{e^2}{4\pi\epsilon_o\hbar c}\right)^4\left(\frac{2m_ec^2}{E}\right)^{L+3/2} \tag{6.8}$$

From these equations the following conclusions are important:

- α depends on Z^3 so for heavier nuclei the electron emission will become more important.
- α will decrease with an increasing transition energy.
- α will increase with increasing multipole order.
- α depends on the electron shell as n^3 so the ratio of $\frac{\alpha_k}{\alpha_l}$ equals to $\frac{1}{8}$ and will be approximately constant (thus independent of the energy).

The behaviour of α for ${}^{152}_{63}$Eu is plotted in figure 6.3. This figure has been drawn based on the values for α as tabulated in [Lederer 1978].

From the equations 6.7 and 6.8 can be seen that the electron conversion coefficient is determined by the nucleus, the transition mode and the transition energy. This means that knowing the conversion coefficient and transition energy for a given transition in a nucleus of interest, also the transition mode for this transitions can be determined. The conversion coefficient can be obtained in two different ways:

- One can measure a γ and an electron spectrum. Dividing the peak yield for a certain γ ray of interest and the yield of the corresponding electron peak gives α. The disadvantage is that one has to correct for the efficiency of the electron and γ detector.
- If the electron spectrum has a good resolution a better way is to determine the $\frac{K}{L}$ ratio, this is the ratio of the K electron yield relative to the L electron yield. This value is insensitive to the efficiency so from that point of view more accurate, however often the L peaks have not good statistics which makes this method generally less accurate.

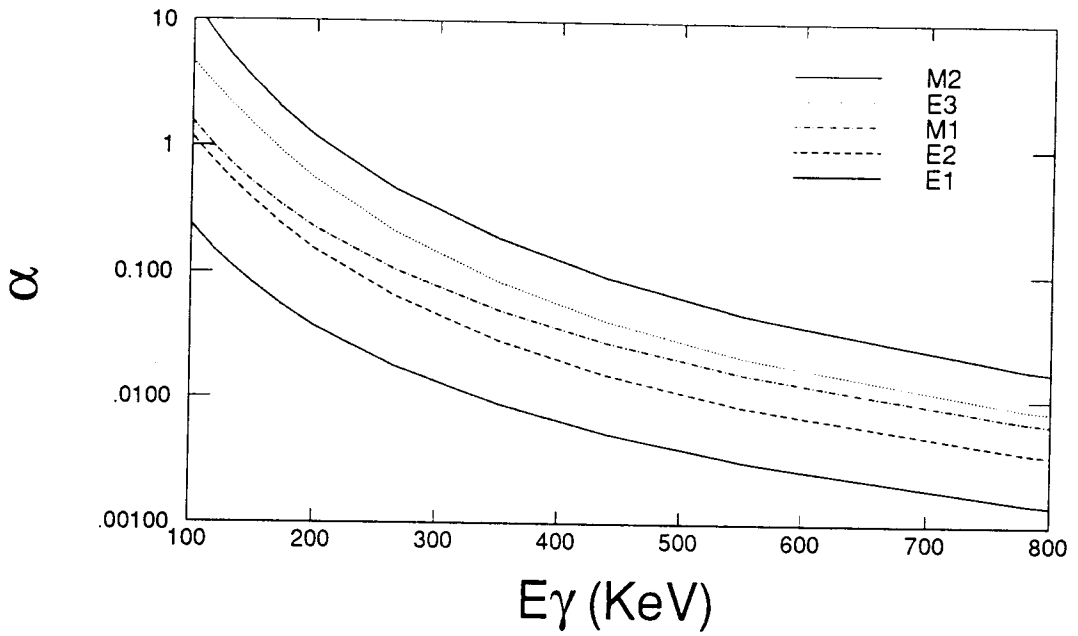

Figure 6.3: α *vs* γ *energy*

Now if the transition mode is known for a certain transition also the parity change between the two levels involved is known.

$\Delta\pi = +1$: even electric, odd magnetic
$\Delta\pi = -1$: odd electric, even magnetic

If now the parity for one of the levels is known, the parity for the other level will be induced.

Chapter 7

Experimental setup

As already described in the introduction the reactions used to produce the Europium nuclei are:

$$^{148}_{60}\mathrm{Nd}(\ ^{7}_{3}\mathrm{Li} + 50\ \mathrm{MeV}, 5\mathrm{n})\ ^{150}_{63}\mathrm{Eu}$$
$$^{148}_{60}\mathrm{Nd}(\ ^{7}_{3}\mathrm{Li} + 40\ \mathrm{MeV}, 4\mathrm{n})\ ^{151}_{63}\mathrm{Eu}$$

The $^{148}_{60}$Nd target had a thickness of 250 μg/cm^2 and was placed under an angle of 30° relative to the beam. This angle was chosen to increase the thickness of the target for the beam. The original plan was to use a thicker target but the thicker Neodymium target was badly oxidized because the container for the thick target was not air tight.

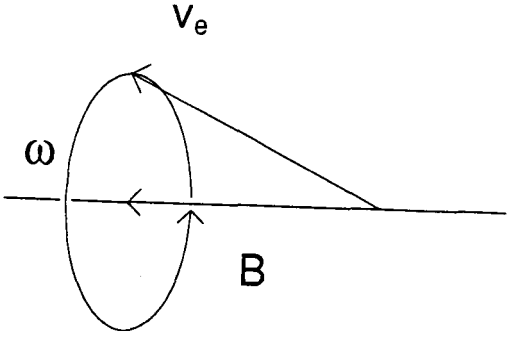

Figure 7.1: *An electron that enters a magnetic field will start to spiral around the axis of the field.*

The main part of the experimental setup was a Kleinheinz magnetic lens (reference [Lagrange 1988]). This lens is based on the principle that electrons entering an axial magnetic field, where the motion of the electron is under

a small angle to the axis, will start to spiral around the axis of this field (see figure 7.1). The spiraling track the electron will follow is determined by the strength of the magnetic field, the angle of entry and the energy of the electron.

$$m\omega^2 r = q\overline{v} \times \overline{B} \tag{7.1}$$

Here ω is the spiraling frequency and r the radius of the spiral. If one now inserts a mechanical spiral (a big corkscrew) in this magnetic field, only those electrons whose path matches the spiral will be able to pass through. Behind this spiral a SiLi detector is placed, with a thickness of 4mm and 600 mm^2 in area, to detect the electrons that pass through the spiral. In this way a very low background electron detector has been made. The possibility to sweep the magnetic field has been built in to make scanning of an energy range possible. Furthermore a germanium detector is used to detect γ rays. This detector is surrounded by a BGO (BGO stands for Bismuth Germanium Oxide, which is a scintillation crystal) for Compton suppression. Finally a multiplicity BaF_2 filter is present. The total setup can be seen in figure 7.2. A brief summary of the above mentioned features will be given.

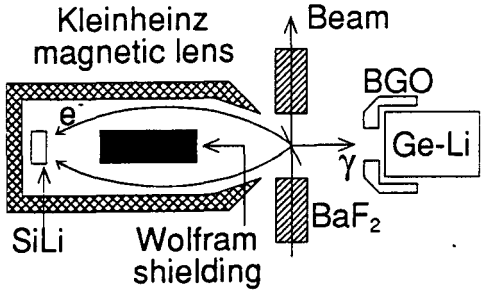

Figure 7.2: *Experimental setup used in Orsay*

- To measure conversion electrons an electron detector is needed. In Orsay a high quality electron detector is available in the form of a Kleinheinz magnetic lens.
- The multiplicity filter is useful in decreasing contaminant (non interesting) reaction channels.
- The very good ^7Li beam coming from the Tandem also is a big advantage for this experiment.

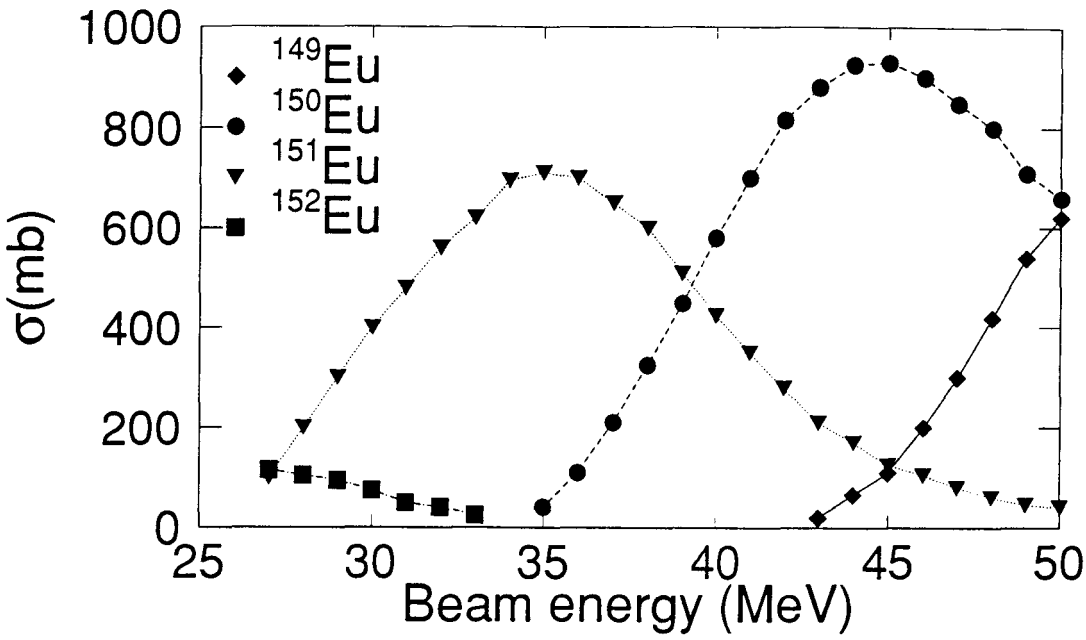

Figure 7.3: *Cross section vs. beam energy for the different Europium isotopes*

The actual experiment can be split in four parts. First of all because there are two different nuclei studied (^{150}Eu and ^{151}Eu). The optimum beam energy to produce these nuclei has been evaluated with the help of CASCADE, a program which can calculate excitation functions. The output of CASCADE is shown in figure 7.3. From experience is known that the predictions CASCADE makes for the beam energy are in the order of a few MeV too low. So the decision was made not to run at 35 MeV and 45 MeV but to use higher beam energies of 40 MeV and 50 MeV. Later on some attention will be paid to the fact that it is not possible to produce only one type of nucleus, the neighboring nuclei will also be present. The second reason for splitting the experiment in parts is the difference in conversion coefficients for low and high energies. Looking at figure 6.3 one can see that the conversion coefficients, for the same type of transition, are much higher at low energies than at high energies. Because of this one can split the experiment

in a low energy part (50 to 500 keV) and a high energy part (400 to 1000 keV), where for the low energy part a smaller run time is needed to get the same statistics. The energy range of this low and high energy region is set with the help of the sweeping field. In figure 7.4 an example of a low energy spectrum and a high energy spectrum are shown.

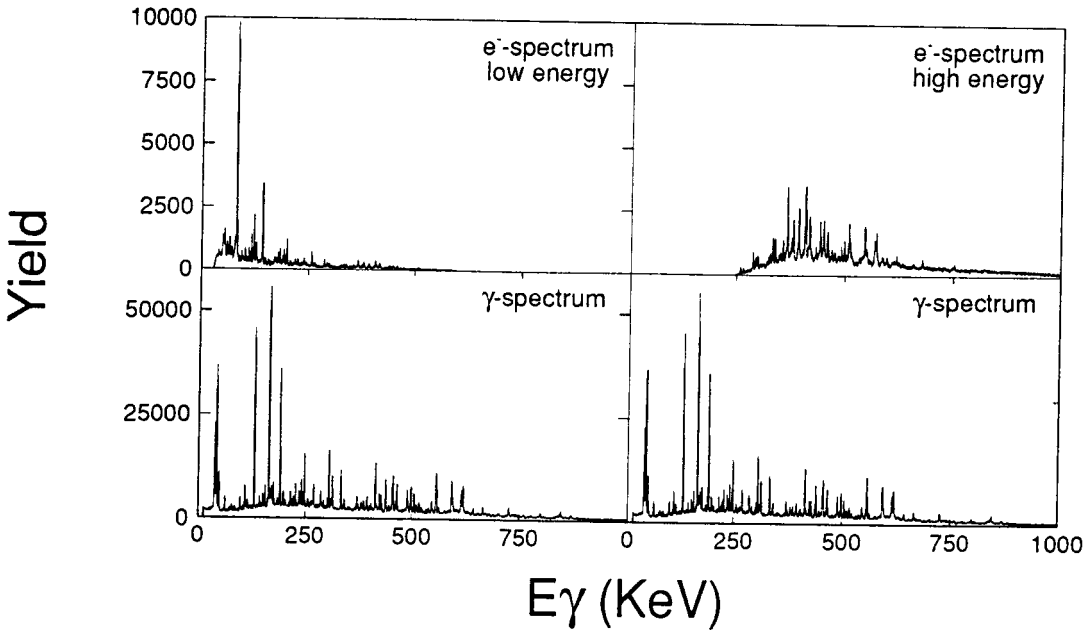

Figure 7.4: *Low and high energy electron spectrum plus the obtained γ spectrum*

From the two electron spectrum a few things about the setup can be shown.

- The effect of the sweeping is rather clear. The low energy spectrum has no counts below 50 keV and no counts above 500 keV, while the high energy spectrum has no counts below 250 keV and above 800 keV.
- The low energy background is not only reduced because of the sweeping range but also because of the so-called banana gate (figure 7.5). When

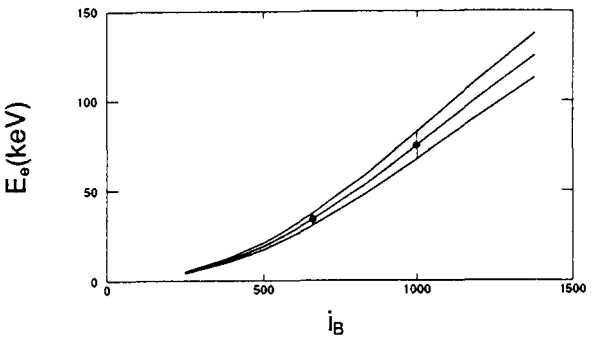

Figure 7.5: *The banana gate, showing the acceptance of the lens*

a certain energy is set by the magnetic field only those electron that have an energy within 10% of the set energy are accepted. So electrons that are able to pass the magnetic lens via scattering have most likely an energy that does not fall within the gate. Therefore these events are rejected and do not contribute to the background. In the figure the selected energy is the middle line and the acceptance is given by the upper and lower line (for two points this has been illustrated).

- Also the prove is given for the earlier made statement that at lower energies the conversion rate is much higher than at higher energies. Especially in the low energy spectrum this is shown.

- Finally it should be noted that the spectra do not have the same run times so no quantitave conclusions can be drawn from these spectra.

Chapter 8

Analyses and Results

Before showing the results of the experiment, the data taking and analyses methods will be shown. After that the results will be presented.

8.1 Analyses

The data was accumulated on a personal computer and later on transported to a vax system. Analyses of the data was done with help of a peak fitting program (GELIFT, designed by D.C. Radford at the Chalk River Nuclear Laboratories, Ontario Canada). This program made it possible to fit besides straight forward Gaussians also tails to peaks, which is rather important when fitting electron spectra because electron peaks generally have a low energy tail due to energy loss in e.g. the detector window or the target. The equation used to fit the electron peaks consists of three parts, the actual Gaussian and main part of the peak, a skewed Gaussian to correct for trapping and energy loss effects and a step function at the low energy side of the peak.

$$Y = constant \cdot EXP(\frac{x-c}{\beta}) \cdot ERFC((\frac{x-c}{\sqrt{2}\cdot\sigma}) + (\frac{\sigma}{\sqrt{2}\cdot\beta})) \qquad (8.1)$$

Here ERFC is the complement of the error function, x is the channel number and c and σ are respectively the centroid and standard deviation of the Gaussian. β is the decay constant of the exponential so it corresponds to the skewness of the Gaussian. The program now has the ability to fit these parameters if the approximate location of the peak is given, also the FWHM

(Full Width Half Maximum) will be fitted. However especially the electron spectra contain so many peaks that it is hard to judge whether a fit is good or whether there are contaminating peaks. To reduce this problem a little bit it is possible to enter a width calibration. So one takes a number of "clean" peaks, determines the width and fits these with a linear function. The function obtained then is an input parameter of the fitting routine so the program will fit with fixed FWHM's. From this program values for the centroids and the peak yields are obtained. Since the difference between the electron peaks and the γ peaks is fixed (see equations 6.4 and 6.5) one can now take the list of fitted peaks for both the γ and the electron spectrum and look for those transitions for which both peaks are detected. The only thing that still stands in between the data and the internal conversion coefficient is the detection efficiency. This efficiency can be described as three parts:

$$Eff = constant \cdot \frac{Eff_e}{Eff_{gamma}} \tag{8.2}$$

$$Eff_\gamma = ((a + b \cdot x)^{-G} + (d + e \cdot x)^{-G})^{\frac{-1}{G}}$$

$$Eff_e = \sqrt{(\frac{E_e}{511})^2 + 2 \cdot \frac{E_e}{511}}$$

x is here $\log(E_\gamma)$. See figure 8.1 for the used efficiencies.

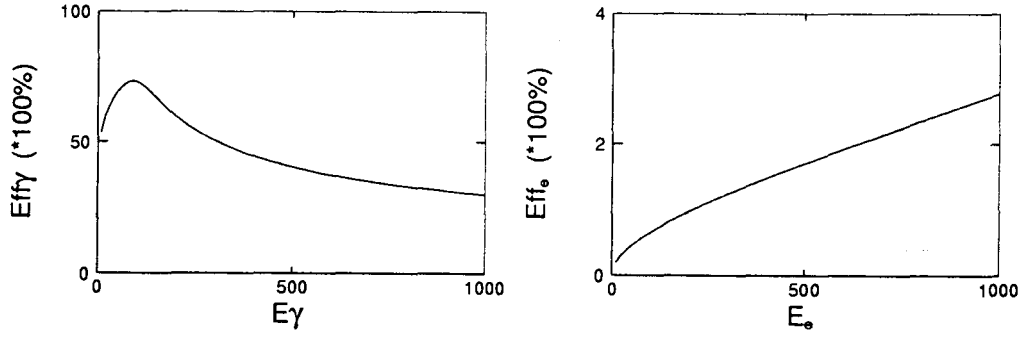

Figure 8.1: γ *and electron detection efficiency*

The efficiency for the detection of γ's is based on two linear efficiencies, one for the low energy region and one for the high energy region. G is the

smoothing parameter between the two regions. For the electron detection efficiency the ratio $\frac{\Delta p}{p}$ is used. Finally a *constant* is included which is used to normalize between γ detector and electron detector. To determine now the conversion coefficients the ratio of the electron peak intensity (I_e) and γ peak intensity (I_γ) is taken multiplied with the efficiency.

$$\alpha_k = constant \cdot \frac{Eff_e}{Eff_\gamma} \cdot \frac{I_{e_k}}{I_{gamma}} \tag{8.3}$$

The *constant* is determined from a transition for which the conversion coefficient is well known, mostly a strong E2 transition.

8.2 Results

In this section the results are presented from the internal conversion experiment. First attention will be paid to the γ spectra obtained for ^{150}Eu and ^{151}Eu, later on the results for the conversion coefficients will be presented.

Looking at the measured γ spectrum (figure 8.2) there are some features that need to be noted.

- From figure 7.3 can be seen that at a given beam energy not only the nucleus with the highest cross section will be produced but also the neighboring ones. Looking at figure 8.2 this indeed can be seen. The strongest peak in the ^{151}Eu spectrum (305.9 keV) is clearly present in the spectrum for ^{150}Eu and vice versa the 190.5 keV peak of ^{150}Eu is clearly visible in the ^{151}Eu spectrum. This has a very important consequence for the analyses. One should not only be careful for doublets within one nucleus but it might also be that γ rays from the neighboring nucleus have the same energy as γ rays from the nucleus of interest.

- Below 50 keV some very strong peaks are visible. These peaks are due to X ray emission from the nuclei created. When looking in the low energy regions one has to be careful for tails from these peaks.

- Another typical feature of a γ spectrum can be seen in the ^{151}Eu spectrum. There are peaks at energies: 305.9 keV, 454.9 keV, 546.0 keV, 614.7 keV, 671.9 keV and even further. These are peaks belonging to

a rotational band of ^{151}Eu. In the ideal case the energy difference between two cascading γ rays is a constant. This constant can be derived from equation 6.2 and is equal to:

$$\Delta E_\gamma = E_\gamma(I) - E_\gamma(I-2) = \frac{8\hbar^2}{2J} \tag{8.4}$$

Looking at the above mentioned peaks in the γ spectrum, of which is presumed that they make up a rotational band, it can be seen that the energy difference is not a constant. The reason can be found in the Moment of Inertia J which in the ideal case is presumed to be constant but actually depends on the angular momentum. With increasing angular momentum the Moment of Inertia will increase so the ΔE_γ will decrease.

The obtained internal conversion coefficients are shown if figure 8.3, figure 8.4 and figure 8.5. The electron spectra for ^{150}Eu and ^{151}Eu as well as the tables containing the conversion coefficients can be found in appendix A and appendix B. From the obtained internal conversion coefficients the following conclusions can be drawn.

- For both nuclei a large amount of E2 transitions can be seen. This is a clear hint to the presence of rotational bands.
- Also for both nuclei one can observe E1 and M1 transitions. Specially the E1 transitions are very interesting because an E1 transition implicates a parity change. Remembering the discussion about the two rotational bands with opposite parity which are sometimes present in octupole deformed nuclei, the E1 transitions might form the connections between such bands.
- For the case of ^{150}Eu also the L conversion coefficients are shown (figure 8.4). This was done because of the interest in a γ ray with an energy of 60.8 keV. This transition has until now not been seen although one is almost sure that it is present. The difficulty in detecting this transitions is first of all in the γ detection. Not all γ detectors can detect at these low energies. The second reason is in the energy of the conversion electron. In the case of K conversion the electron energy would be 20 keV which is almost impossible to see. So one has to look for the L

conversion which has lower intensities than the K conversion but at an acceptable energy to detect (52.7 keV). Because of the quality of the electron detector used in this experiment it was possible to detect the L conversion electron and to determine the transition mode for this transition.

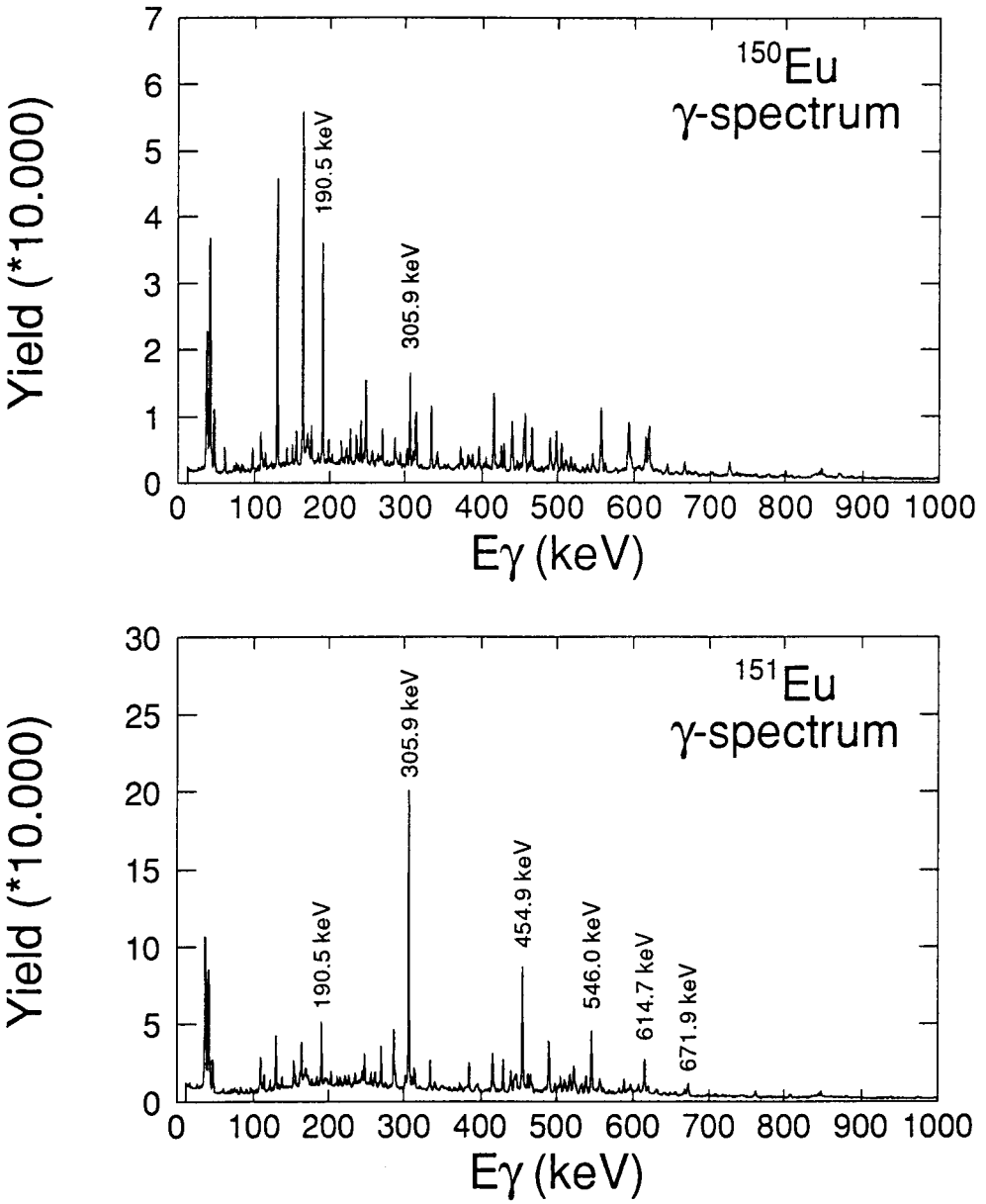

Figure 8.2: *γ spectrum for ^{150}Eu and ^{151}Eu*

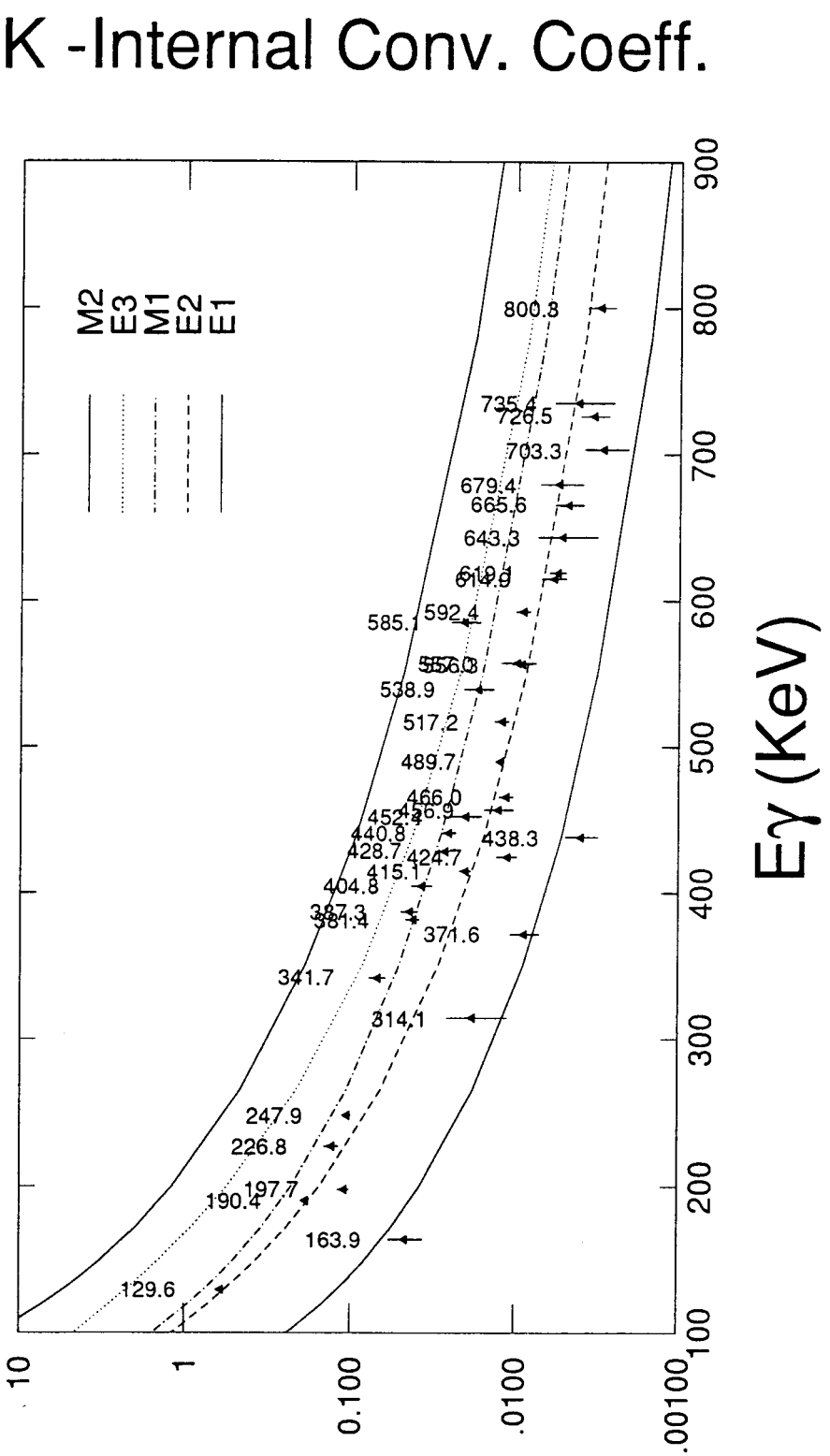

Figure 8.3: *K conversion coefficients for* ^{150}Eu

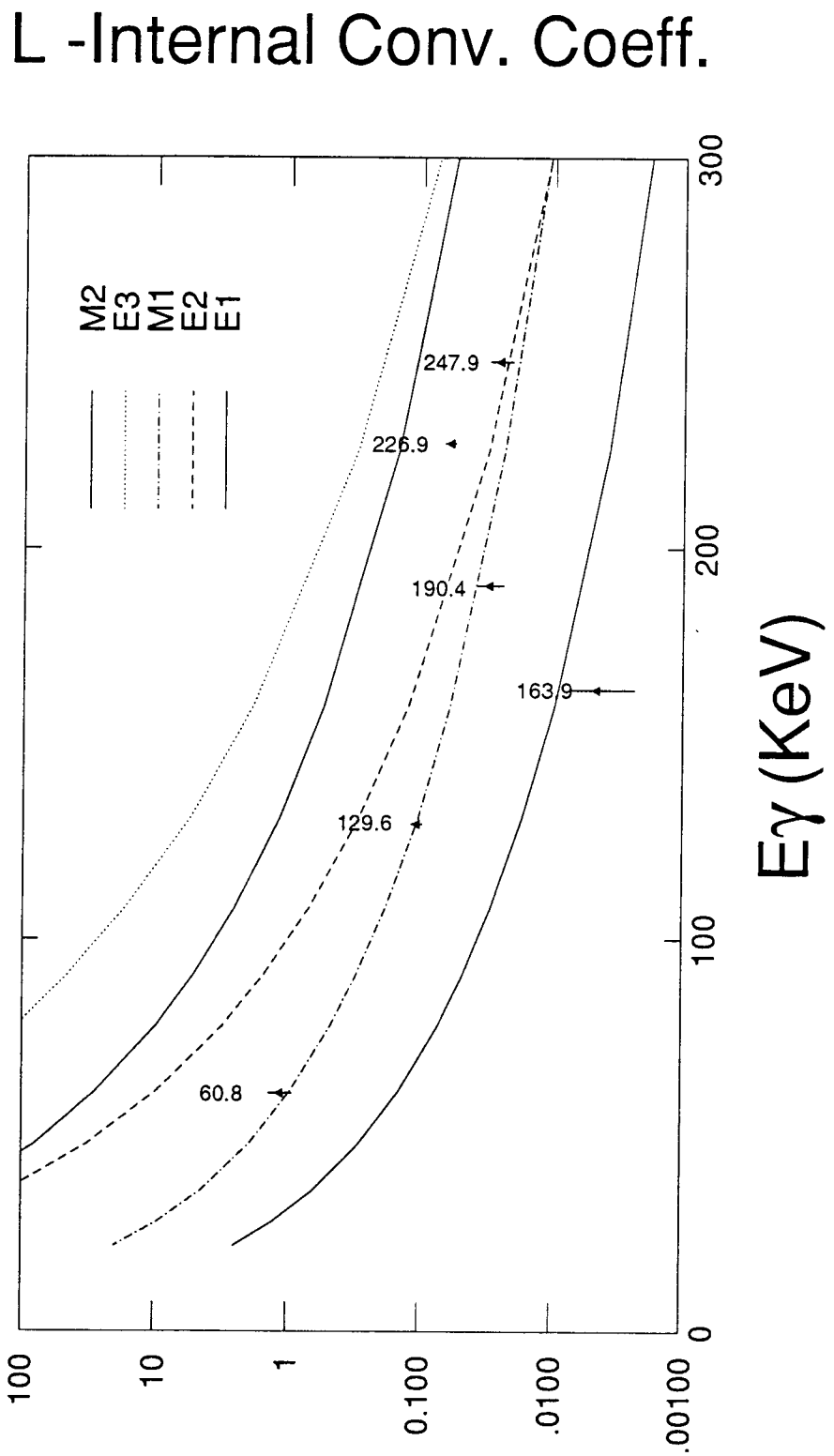

Figure 8.4: *L conversion coefficients for* ^{150}Eu

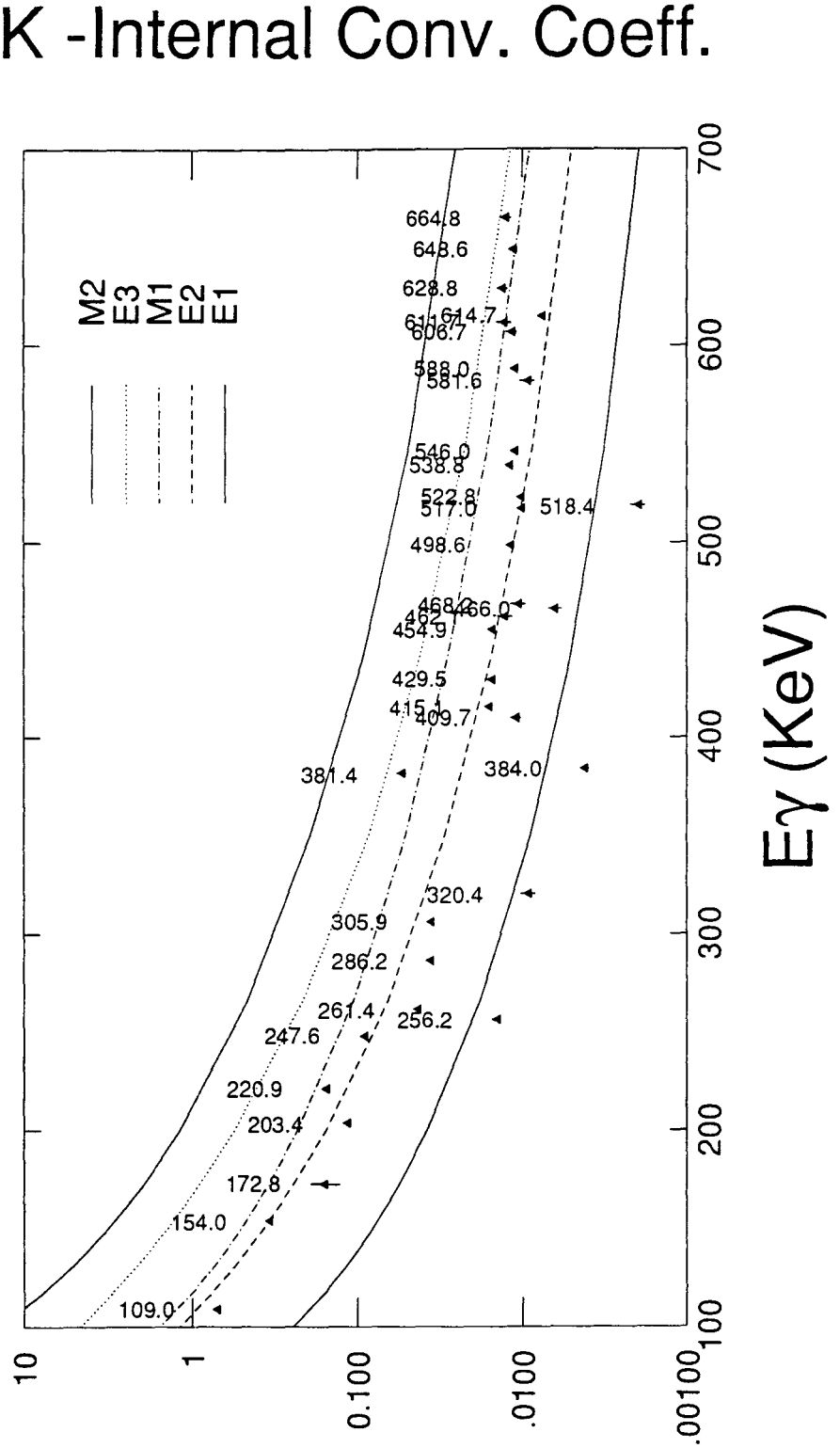

Figure 8.5: *K conversion coefficients for* ^{151}Eu

Chapter 9

conclusions

At this point it is necessary to stress that the results from this experiment are only a part of a big experiment trying to determine the structure of the Europium nuclei. This means that the presented results and level schemes are preliminary. The level schemes can be found in Appendix A and Appendix B. The conclusions that can be drawn from the analyses are:

- The most important conclusion that can be drawn is that the two studied Europium nuclei are not or very little octupole deformed. Looking at the conversion coefficients only very few E1 transitions are seen compared to the number of E2 transitions. As noted before (chapter 6) in the case of octupole deformed nuclei the E1 and E2 strength is approximately the same and because the E1 transitions couple two rotational bands they should also in amount be roughly the same.

- Looking at the level schemes (see appendix A and B) one can see that there are a lot of transitions between bands. These have been found to be M1 transitions. So there is no parity change between the bands.

- Specially the lines at lower energies are very important and show the advantage of this experiment. Because of the low background in using this lens it has become possible to see very low energetic electrons. The best example for this is the 69.6 keV line that has been measured for the first time.

Bibliography

[Barneoud 1983] D. Barneoud et.al.
High spin states in the transitional odd-odd nuclei ^{150}Eu and ^{152}Tb.
Z.Phys A 314, 69-79(1983)

[Blatt 1966] J.M. Blatt and V.F. Weiskopf
Theoretical Nuclear Physics
John Wiley & Sons. Inc.
New York 1966

[Ejiri 1989] H. Ejiri and M.J.A. de Voigt
Gamma-ray and electron spectroscopy in nuclear physics
Clarendon Press
Oxford 1989

[Klinken 1986] J. van Klinken
Mini Orange sketches
KVI 122i (internal report)
Groningen 1986

[Krane 1987] K.S. Krane
Introductory nuclear physics
John Wiley & Sons. Inc.
Oregan state university 1989

[Lagrange 1988] J.M. Lagrange et.al.
Spectroscopic study of short lived, high spin isomers, through the recoil method
NIM A271, 527-542 (1988)

[Lederer 1978] C.M. Lederer
Table of Isotopes
John Wiley & Sons. Inc.

[Segre 1959] E. Segre, Editor
Experimental Nuclear Physics (Volume III)
John Wiley & Sons. Inc.
New York 1959

[Siegbahn 1964] K. Siegbahn
Alpha-, Beta- and Gamma-ray spectroscopy (Volume II)
Chapter XVI, Theory of Internal Conversion by M.E.Rose
North Holland Publishing Company
Uppsala 1964

[Soramel 1983] F. Soramel-Stanco et.al.
A 45 ns isomer in the doubly odd ^{150}Eu nucleus
Z.Phys A 314, 127-133 (1983)

[Steenbergen 1989] T. Steenbergen
The nuclear structure of ^{148}Europium
Thesis doctoral examination
Groningen 1989

Acknowledgements

Making this report would not have been possible without the help of some people whom I would like to thank at this point for their time and help.

Jose Bacelar who always took the time to give me advice and explain al those things to me I did not understand.

Jan Jongman with whom I went two times abroad for an experiment, first to Orsay and later to Debrecen. The discussions with him about non physics matters were just as interesting as the discussions about physics.

Attilla Krasznahorkay and with him al the people in Debrecen who helped with the experiment and did not get annoyed with us because the experiment failed.

My family and Ineke who were always prepared to listen to the things I did although the work was not always that interesting.

The OIO's working at the KVI who were always prepared to give advice when I had some questions. Especially **Henk Leegte** who kept on answering my questions about computers.

Prof. M.J.A. de Voigt who made it possible for me to work at the KVI. He played a very important role in my study because also an earlier research done in Japan was only possible thanks to him.

Maybe I forgot to mention people by name here. This is not because I am not grateful to them but because every now and then something might have slipped my mind.

List of Figures

List of Tables

Appendix A

^{150}Eu

$E\gamma$	E_{e_k}	$\alpha_k \cdot 10^2$	$\alpha_l \cdot 10^2$	tt
60.8			115.(20)	M1
129.6	81.1	61.(1)	11.(1)	M1
163.9	115.4	4.7 (5)	0.5 (2)	E1
190.4	141.9	19.(1)	3.1 (3)	M1
226.8	178.3	13.(1)	6.2 (1)	M1
247.9	199.4	11.(1)	2.6 (3)	M1
314.1	265.6	1.8 (3)		E1
341.7	293.2	6.9 (6)		M1
371.6	323.1	8.9 (8)		E1
381.4	332.9	4.2 (2)		M1
387.3	338.7	4.4 (3)		M1
404.8	356.3	3.7 (3)		M1
415.1	366.6	2.0 (1)		E2
424.7	376.2	1.1 (1)		E2
428.7	380.3	2.9 (1)		M1
438.3	389.8	0.40 (4)		E1
440.8	392.3	2.5 (2)		M1
452.4	403.9	2.0 (4)		M1
456.9	408.4	1.3 (2)		E2

$E\gamma$	E_{e_k}	$\alpha_k \cdot 10^2$	$\alpha_l \cdot 10^2$	tt
466.0	417.5	1.2 (1)		E2
489.7	441.2	1.3 (1)		E2
517.2	468.7	1.2 (1)		E2
538.9	490.4	1.7 (4)		M1
556.3	507.8	0.93 (9)		E2
557.0	508.5	0.99 (9)		E2
585.1	536.6	2.1 (3)		M1
592.4	543.9	0.91 (5)		E2
614.9	566.4	0.60 (6)		E2
619.1	570.6	0.56 (5)		E2
643.3	594.8	0.5 (2)		E2
665.6	617.1	0.48 (7)		E2
679.4	631.9	0.55 (9)		E2
703.3	655.8	0.30 (8)		E2
726.5	676.0	0.34 (6)		E2
735.4	686.9	0.42 (7)		E2
800.3	751.8	0.31 (6)		E2

Table A.1: *Conversion coefficients for* ^{150}Eu

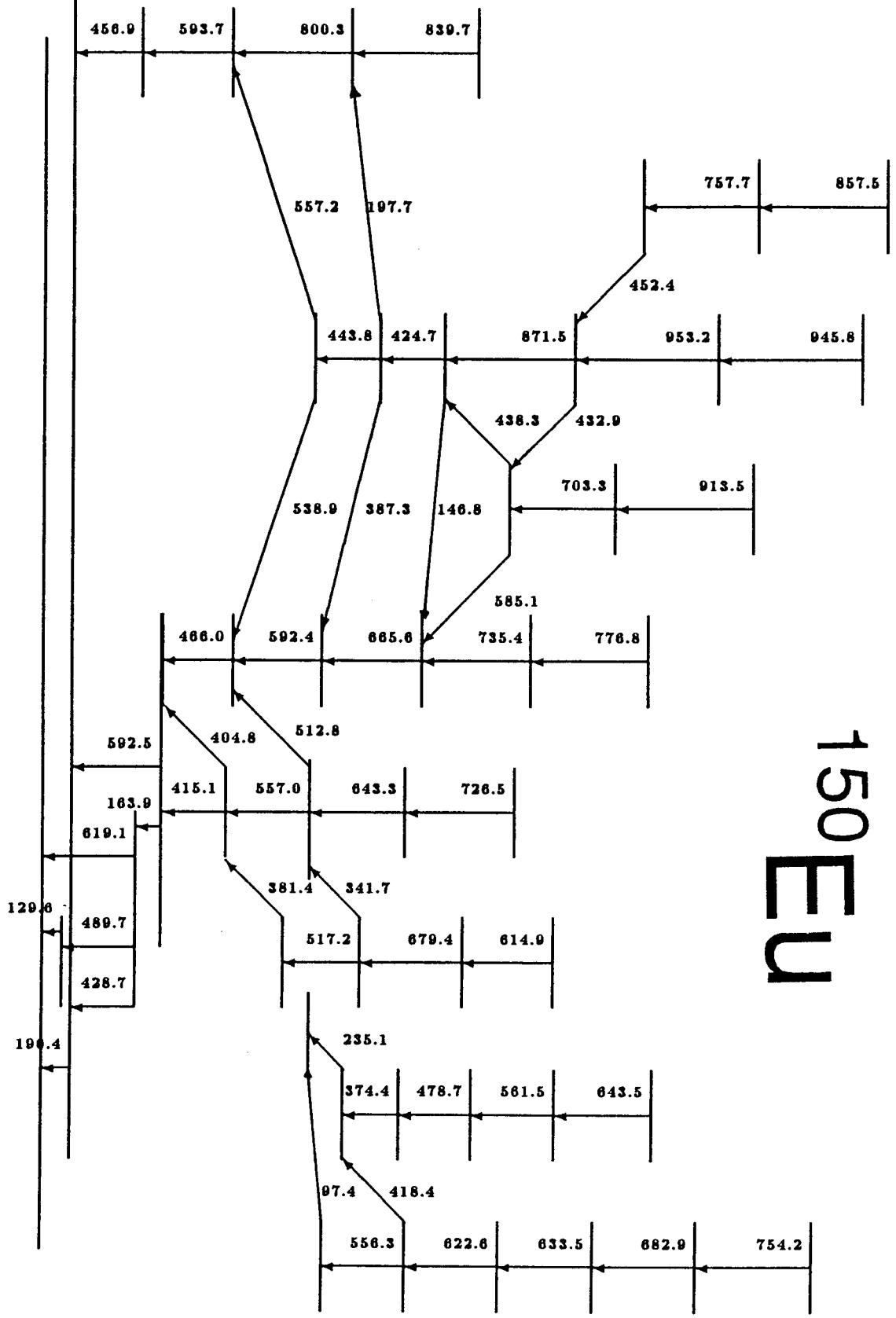
456.9
593.7
800.3
839.7
557.2
197.7
757.7
857.5
452.4
443.8
424.7
871.5
953.2
945.8
438.3
432.9
703.3
913.5
538.9
387.3
146.8
585.1
466.0
592.4
665.6
735.4
776.8
512.8
404.8
592.5
415.1
557.0
643.3
726.5
163.9
619.1
381.4
341.7
129.6
489.7
517.2
679.4
614.9
428.7
190.4
235.1
374.4
478.7
561.5
643.5
97.4
418.4
556.3
622.6
633.5
682.9
754.2
150Eu

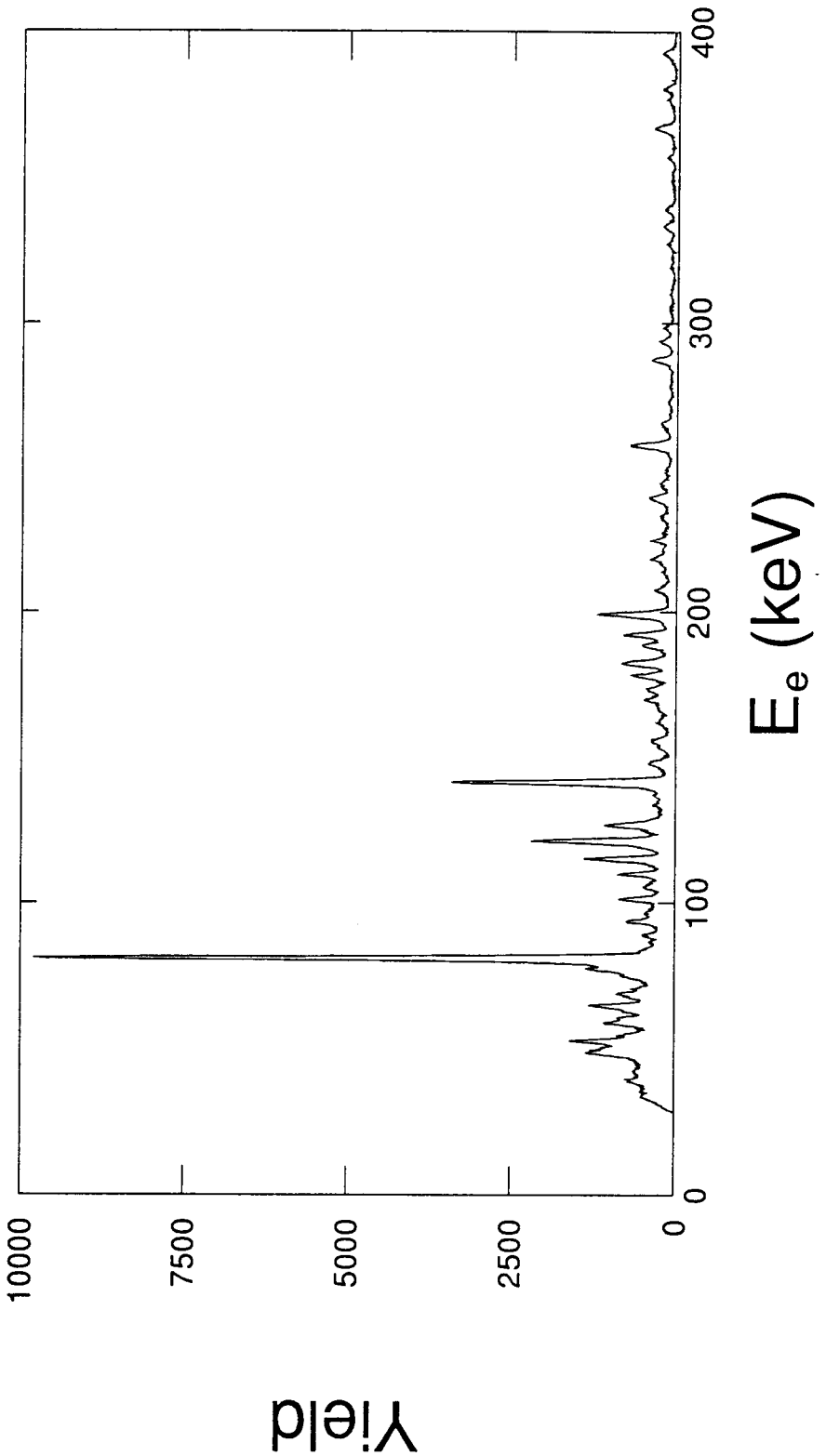

Figure A.2: *Electron conversion spectrum for* ^{150}Eu

Appendix B

^{151}Eu

$E\gamma$	E_{e_k}	$\alpha_k \cdot 10^2$	$\frac{\alpha_k}{\alpha_l}$	tt
109.0	60.5	71.(1)	5.3 (3)	E2
154.0	105.1	33.(3)	5.6 (5)	E2
172.8	124.0	15.(20)		E1
203.4	154.8	11.(1)		E2
220.9	172.8	15.(1)		M1
247.6	199.3	9.1 (4)		E2
256.2	207.6	1.4 (1)		E1
261.4	213.3	4.3 (3)	1.5 (4)	E2
286.2	237.9	3.6 (2)		E2
305.9	257.6	3.6 (1)		E2
320.4	271.8	0.93 (9)		E1
381.4	332.5	5.4 (4)		M1
384.0	335.4	0.42 (3)		E1
409.7	361.3	1.1 (1)		E2
415.1	366.7	1.6 (1)		E2
429.5	381.0	1.5 (1)	4.4 (4)	E2
454.9	406.6	1.5 (1)		E2
462.1	413.8	1.3 (1)		E2
466.0	417.6	0.64 (9)		E1

$E\gamma$	E_{e_k}	$\alpha_k \cdot 10^2$	$\frac{\alpha_k}{\alpha_l}$	tt
468.2	419.7	1.1 (6)		E2
498.6	449.9	1.2 (8)		E2
517.0	468.5	1.0 (1)		E2
518.4	470.1	0.2 (1)		E1
522.8	474.6	1.0 (1)		E2
538.8	490.4	1.2 (1)		M1
546.0	497.7	1.1 (1)		E2
581.6	533.2	0.9 (1)		E2
588.0	539.9	1.1 (2)		M1
606.7	558.3	1.2 (4)		M1
611.7	564.0	1.3 (2)		M1
614.7	566.4	0.77 (2)		E2
628.8	580.6	1.3 (3)		E2
648.6	600.1	1.1 (1)		M1
664.8	616.1	1.3 (4)		M1

Table B.1: *Conversion coefficients for* ^{151}Eu

^{151}Eu

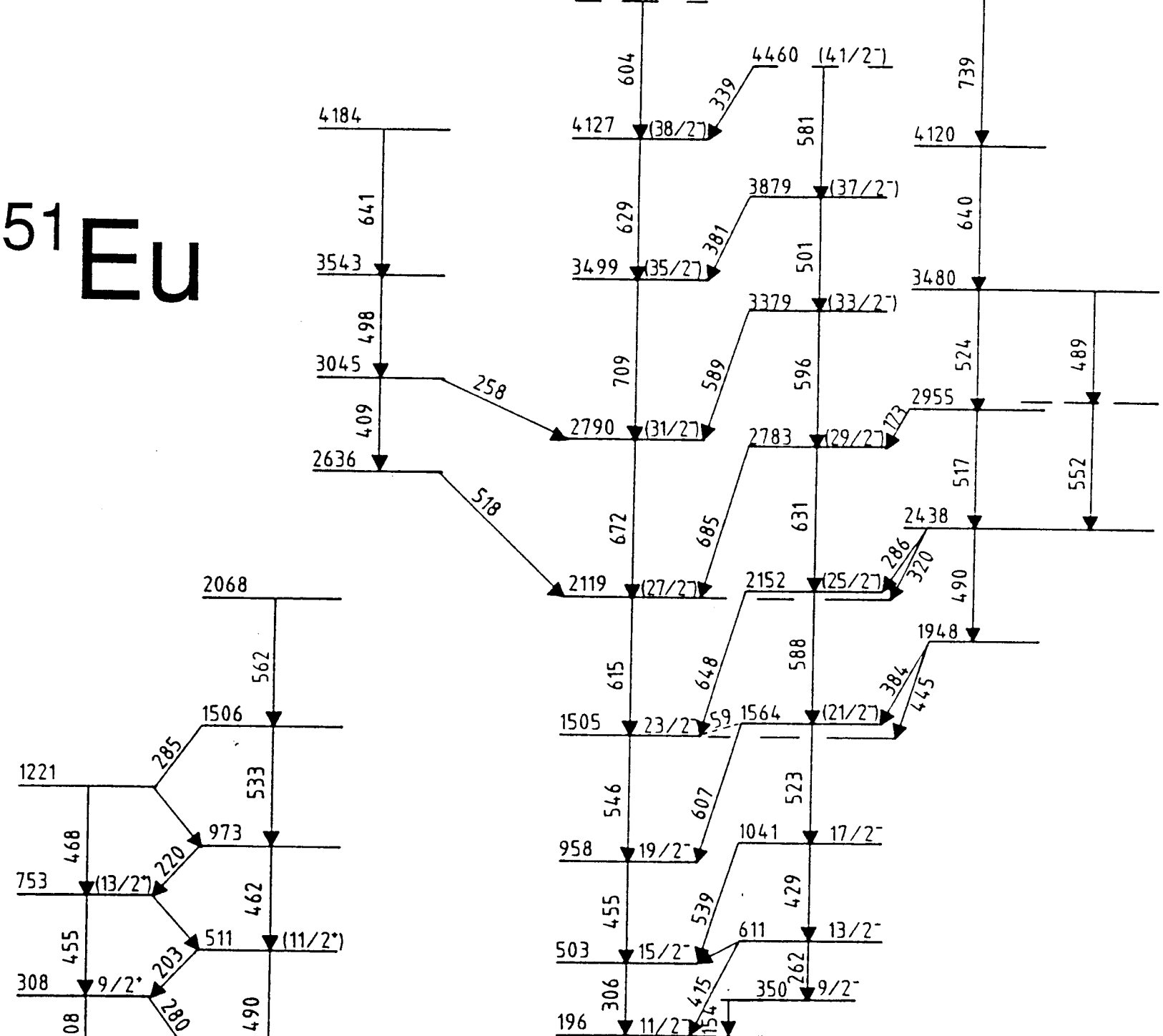
4460 (41/2⁻)
4184
4127 (38/2⁻)
4120
3879 (37/2⁻)
3543
3499 (35/2⁻)
3480
3379 (33/2⁻)
3045
2955
2790 (31/2⁻)
2783 (29/2⁻)
2636
2438
2119 (27/2⁻)
2152 (25/2⁻)
2068
1948
1506
1505 23/2⁻
1564 (21/2⁻)
1221
973
958 19/2⁻
1041 17/2⁻
753 (13/2⁺)
511 (11/2⁺)
503 15/2⁻
611 13/2⁻
308 9/2⁺
350 9/2⁻
196 11/2⁻
604
339
581
739
641
629
381
501
640
498
709
589
596
524
489
258
409
123
517
552
672
685
631
286
320
518
490
562
615
648
588
384
445
285
533
546
607
523
468
220
462
539
429
455
203
455
306
415
262
280
490
154
308

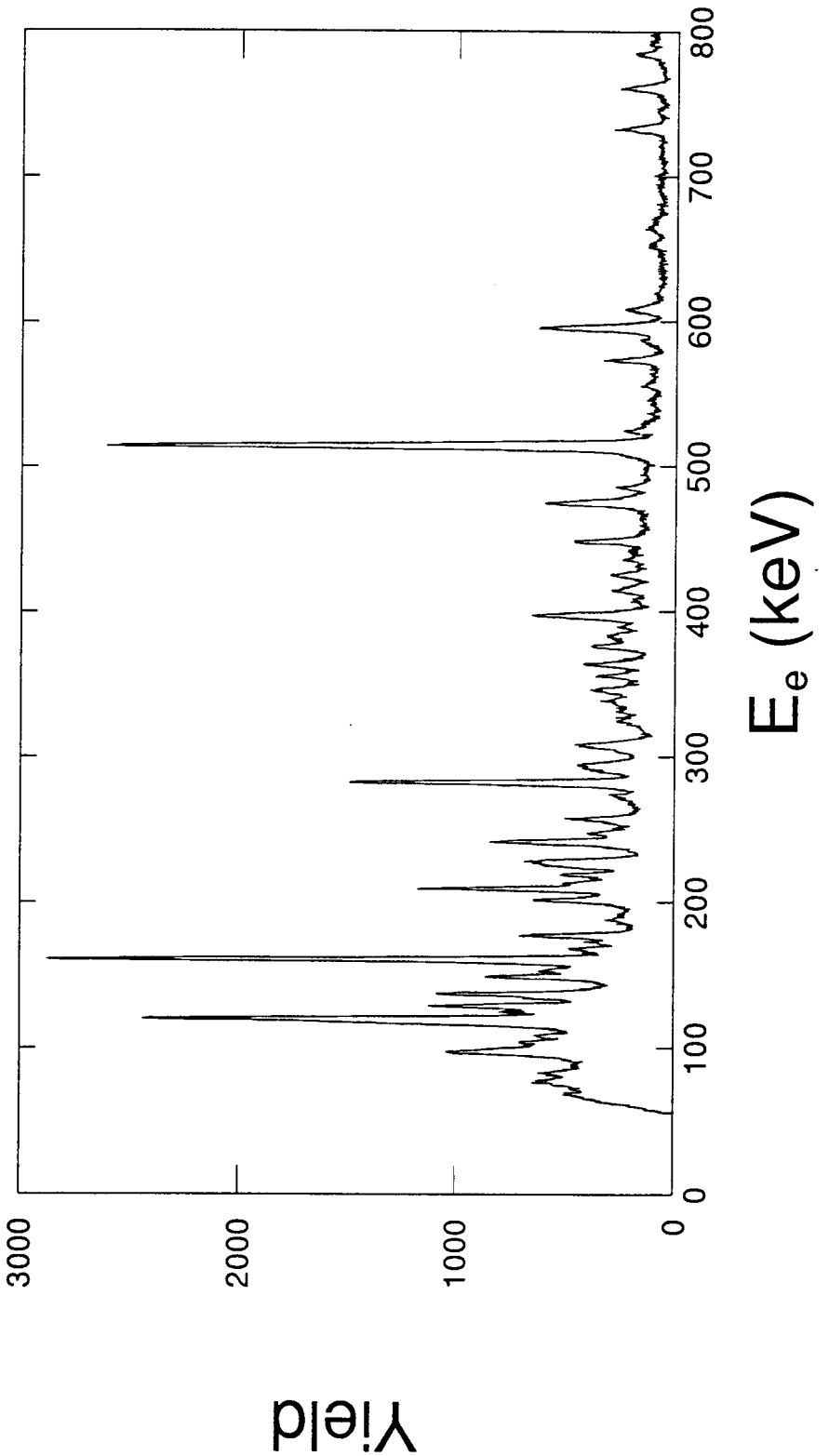

Figure B.2: *Electron conversion spectrum for* ^{151}Eu

Appendix C

Programs

For the analyses some special programs have been written. They have not been integrated yet but this might be a good improvement. The best procedure to analyse the data and obtain a spectrum is shown in figure C.1.

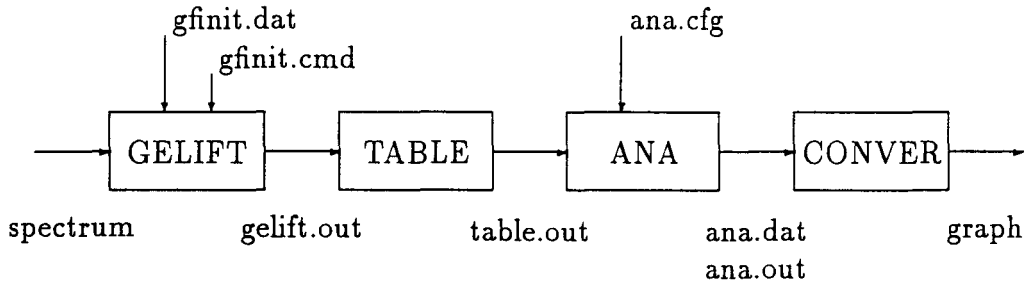

Figure C.1: *Analyses programs*

The files below the flow diagram are transported between the different programs and the format of them is adapted so there should appear no problems. The files above the flow diagram are needed to run the programs and contain vital information. Now some explanation will be given about the different programs.

- GELIFT is already described in detail in section 8.1. At this point only examples for the input files will be shown (figure C.2 and figure C.3).

```
0.0,0.0,0.0,0.0,0.0   ; ← A,B,C,D,E Starting skewed Gaussian
0,0,0                 ; ← 0/1 for r, β, step fixed/free
2.670,3.202,1.921     ; ← F,G,H Starting widths
0,0                   ; ← 0/1 for absolute- and relative widths fixed/free.
```

Figure C.2: *Example for gelift.dat*

```
SP EGF2.GF2   ; ← Read spectrum EGF2.GF2
EC            ; ← Load energy calibration
Y
Y
1.366,.3559,0 ; ← A,B,C from energy calibration
NY-2          ; ← Set y scale logarithmic
NX 300        ; ← Set x scale 300 channels
CF ERA        ; ← Erase graphics display
DS 1          ; ← Display spectrum
CF END        ; ← End of configuration file
```

Figure C.3: *Example for gelift.cmd*

- TABLE converts the output file from GELIFT into a file table.out that contains the channel, the yield, the FWHM and the energy of the peaks. The last one is only given if the energy was calibrated in GELIFT.

- ANA is the actual analyses program. This program uses as input ana.cfg which is shown in figure C.4

  To start one puts the normalisation factor to 1, after running the program one can normalize on a strong well known line and insert the normalisation factor. The program has the options to give the accuracy of the analyses, which determines the maximum difference between a wanted and a obtained energy. Further more automatic cross scanning of an electron and a γ data set is possible but also manually one can give a γ energy of interest and the program will look whether this energy has been found in the γ spectrum and whether the corresponding

```
eef2ban_le.fit   ; ← Input filename electron data
egf2.fit         ; ← Input filename γ data
.007496          ; ← Normalisation factor
k                ; ← The conversion of interest (k or l)
```

Figure C.4: *Example for ana.cfg*

electron peak has been found in the electron spectrum. The output of ANA are two files, ana.out which gives a table containing the requested γ energy, the found γ energy, the found electron energy and the conversion coefficient. The second file ana.dat contains only the γ energy and the conversion coefficient and is suitable as an input file for CONVER to make a graph.

- CONVER (figure C.5) is a command file that creates a graph as e.g. figure 8.3.

```
$mcom        ; ← Program that makes command file
k            ; ← Plot of K conversion coefficients
k_ec.dat     ; ← Input file
0,0          ; ← xmin,xmax (0,0) means programs choice
0,0          ; ← xmin,xmax (0,0) means programs choice
$@econver    ; ← Run created command file
```

Figure C.5: *Command file CONVER*

It automatically determines the axis and puts at every conversion coefficient also the corresponding energy. The basis of this command file is the program MCOM that makes a command file.

After running these programs the results are present in the file ana.out and in the graph created after running CONVER with ana.dat as input file.

Appendix D

Constants

Speed of light	c	$2.998 \cdot 10^{8} \frac{m}{s}$
Charge of electron	q	$1.602 \cdot 10^{-19} C$
Mass of electron	m_e	$5.486 \cdot 10^{-4} u$
Planck's constant	$\hbar$	$1.055 \cdot 10^{-34} Js$
Fine structure	$\frac{e^2}{4\pi\epsilon_0}$	$1.440 \cdot 10^{8} MeV \cdot fm$